Comparative Studies of RSM, RSM–GA and ANFILS for Modeling and Optimization of Naphthalene Adsorption on Chitosan–CTAB–Sodium Bentonite Clay Matrix

Olaosebikan Abidoye Olafadehan* and Victor Ehigimetor Bello
Department of Chemical and Petroleum Engineering, University of Lagos, Akoka-Yaba, Lagos 101017 Nigeria

Abstract

The aim of this article was to compare the predictive abilities of the optimization techniques of response surface methodology (RSM), the hybrid of RSM–genetic algorithm (RSM–GA) and adaptive neuro-fuzzy interference logic system (ANFILS) for design responses of % removal of naphthalene and adsorption capacity of the synthesized composite nanoparticles of chitosan–cetyltrimethylammonium bromide (CTAB)–sodium bentonite clay. The process variables considered were surfactant concentration, X_1, activation time, X_2, activation temperature, X_3, and chitosan dosage, X_4. The ANFILS models showed better modeling abilities of the adsorption data on the synthesized composite adsorbent for reason of lower % mean absolute deviation, lower % error value, higher coefficient of determination, R^2, amongst others and lower error functions' values than those obtained using RSM and RSM-GA for both responses. When applied RSM, the hybrid of RSM–genetic algorithm (RSM–GA) and ANFILS 3–D surface plot optimization technique to determine the optimal conditions for both responses, ANFILS was adjudged the best. The ANFILS predicted optimal conditions were X_1 = 116.00 mg/L, X_2 = 2.06 h, X_3 = 81.2°C and X_4 = 5.20 g. Excellent agreements were achieved between the predicted responses of 99.055% removal of naphthalene and 248.6375 mg/g adsorption capacity and their corresponding experimental values of 99.020% and 248.86 mg/g with % errors of -0.0353 and 0.0894 respectively. Hence, in this study, ANFILS has been successfully used to model and optimize the conditions for the treatment of industrial wastewater containing polycyclic aromatic compounds, especially naphthalene and is hereby recommended for such and similar studies.

Keywords*: Chitosan, Cetyltrimethylammonium bromide, Bentonite clay, RSM, ANFILS.*

1. Introduction

* Corresponding author. Tel.: +234802-912-9559
E-mail address: oolafadehan@unilag.edu.ng

Manuscript History:
Received 18 June, 2022, Revised 23 June, 2022, Accepted 19 July, 2022, Published 31 October, 2022

https://doi.org/10.33736/jaspe.4749.2022

e-ISSN: 2289-7771

The pollution of the environment and the required timely intervention in bringing desirable panacea for its treatment is still a challenge of great interest globally [1]. One of the dreaded pollutants in water bodies and soil linked to anthropogenic activities is the polycyclic aromatic hydrocarbons (PAHs) because of their prevalence in various segments of the environment as a result of various activities of everyday life typically the incomplete combustion of organic matter of different kinds [2]. PAHs are structurally composed of fused two or more benzene rings and they are generally hydrophobic, non-biodegradable and persistent organic compounds. Their entrance in the body system predisposes humans to cancer and life-threatening health issues because of their carcinogenic, mutagenic, teratogenic and immunotoxicogenic nature. Hence, PAHs have been listed amongst 16 ranked dangerous pollutants by the US Environment Pollution Agency (USEPA) and corroborated by the European Union (EU) [2]. The removal of PAHs from contaminated aqueous solution is quite tasking because they are known to be hydrophobic, thermostable and non-biodegradable [3–4). Thus, the removal of PAHs from industrial wastewaters is an area of key interest to the world at large. There are options employed previously in a bid to treat contaminated aqueous solution containing PAHs, which are sonication, adsorption and biodegradation [5]. For reasons of operational simplicity, cost and ease of obtaining myriads of low-cost adsorbents, the use of adsorption has been widely accepted and it has proved to be efficacious for the removal of PAHs from aqueous solution [6–7]. Cabal et al. [8] investigated naphthalene adsorption onto activated carbons derived from bean pod. Yuan et al. [9] investigated the adsorption of PAHs using serial porous carbons. Iovino et al. [10] fitted the Freundlich isotherm to the single and competitive adsorption of toluene and naphthalene onto activated carbon. Liu et al. [11] investigated the adsorption of naphthalene on coal-based activated carbons. However, recently one of the reputable low-cost adsorbents found in the literature for the effective adsorption of PAHs from aqueous solution are the chitosan and clay minerals [12–13].

Chitosan, as a natural polymer, is currently in the topmost list of the affectionate adsorbents among researchers on account of ease of biodegradation, free corrosion effect, high level of safety handling property, ease of modification for better performance, high adsorption capacity, selectivity and fix for pollutants [14–17]. The use of modified chitosan is on the increase with time. It is necessary to make for the few challenges associated with its performance in carrying out separation process via adsorption, especially with pH factor under consideration. One of the modification processes widely reported in the literature is the gratification method with clay minerals to possess some desirable chemical and mechanical properties. The choice of clay minerals like bentonite clay is linked to its environmental friendliness owing to its non-toxicity, swelling capacity, high adsorption capacity, which is credited to the large presence of amino and hydroxyl groups, high coagulating ability and less cost and extensive availability in certain parts of the world typically in the USA [13, 17–20]. Bentonite clay is formed from the product of devitrification and chemical alteration material of igneous origin [21]. It contains primarily montmorillonite [22–23], secondary of kaolinite and Illite and relatively small proportion of carbonates, tridymite, halloysite, zeolites, iron oxides, quartz, feldspar among few others constituents as it varies from locations of different geographic settings. Bentonite clay is classified among the smectite group attributed with di-octahedral alumina-silicate in its structural frame work due to the much presence of montmorillonite and it is represented with the expression $(Na, Ca)_{0.33}(Al, Mg)_2Si_4O_{10}(OH_2).nH_2O$, as its general formula.

Chitosan and bentonite mineral clay can be used to form a hybrid matrix of desirable qualities and high performance in terms of physical, chemical and mechanical properties [24]. The use of chitosan-bentonite matrix has been reported as a viable adsorbent for the separation of pollutants like heavy metals, dyes compounds, organic compounds, to mention but a few, from aqueous solutions especially those modified with surfactants (such as cetyltrimethylammonium bromide, CTAB, with molecular

formula [$(C_{16}H_{33})N(CH_3)_3$]Br) to enhance interlayer spacing of the bentonite structural frame work and introduce NH_4^+ as functional group in the composite or hybrid adsorbent [25]. In addition, CTAB facilitates adequate interlayer opening for chitosan intercalation [26–27] coupled with the electrostatic attraction of NH_3^+ and the available negative sites bentonite structure [28]. This is important because adsorption of organic molecules onto clay minerals is influenced by the chemical properties of the molecules and its surface properties [29].

In the literature, similar composite materials or organo-modified bentonite clay-chitosan adsorbents have been employed for the treatment of contaminated water in batch and continuous modes. Detailed review of the use of chitosan-bentonite clay for the treatment of contaminated wastewater and its reuse are reported elsewhere [30]. However, adsorption processes in batch mode are presented in Table 1.

Table 1. Chitosan-bentonite clay and organo-modified bentonite clay adsorbent previously used for wastewater treatment

S/N	Adsorbents matrix	Method of preparation	Pollutant	% removal/maximum adsorption capacity, q_{max}	Reference
1	Chitosan/bentonite	Ionic exchange by intercalation	Azo dye	q_{max} =323.6 mg/g at 7293 K	[31]
2	Chitosan/bentonite	Ionic exchange by intercalation	Lead ions	q_{max} =0.425 mol/kg at pH=5.95	[32]
3	Chitosan/bentonite	Cross-linked with glutaraldehyde	Methyl orange	q_{max} =224.8 mg/g at pH=7	[33]
4	Chitosan/bentonite	Ionic exchange by intercalation	Deteriorating transformer oil	Not reported	[34]
5	Chitosan/bentonite	Ionic exchange by intercalation	Cr(VI)	% removal=87.6; q_{max} =133.85 mg/g at pH=3 and 298K	[35]
6	Chitosan/bentonite	Cross-linked	Congo red	q_{max} = 500 mg/g at pH=7 and 298K	[36]
7	Chitosan/bentonite	Cross linking with epichlorohydrin	Amino black 10B	q_{max} =990.1 mg/g at pH=7	[37]
8	Chitosan/bentonite	Ionic exchange by intercalation	Amaranth red	q_{max} =362 mg/g at pH=2	[38]
			Methylene blue	q_{max} =496.5 mg/g at pH=10	
9	Chitosan/bentonite	Cross linked with intercalationpichloro-hydrin (ECH	Tartrazine dye	q_{max} =294.1 mg/g at 320K	[39]
			Malachite green dye	q_{max} =435.0 mg/g at320K	[40]
10	Chitosan/bentonite	Ionic exchange by intercalation	Phenol	q_{max} =12.496 mg/g at pH=7	[41]
11	Chitosan/bentonite	Ionic exchange by	Ammonium	% removal =65 at pH=4	[42]

		intercalation	nitrogen		
12	Chitosan/CTAB)/ bentonite	Ionic exchange by intercalation	Weak acid scarlet	% removal =85; q_{max} = 102 mg/g	[43]
13	Chitosan/bentonite	Cross-linked with acrylic acid	Methylene blue	q_{max} = 2000-2500 mg/g at 298–313K	[44]
14	Bentonite/N-2-hydroxypropyl trimethyl ammonium chloride chitosan (HACC)/CTAB	Ionic exchange by intercalation	Phenol	% removal =82.1; q_{max} = 7.12 mg/g at pH=12 and 293K	[45]
15	Chitosan-g-itaconic acid/bentonite	Cross-linked with ammonium persulfate (APS)	Methylene blue	q_{max} = 500 mg/g at pH=6	[46]
	Chitosan/bentonite			q_{max} =81.818 mg/g at pH=7	
16	Chitosan/bentonite	Cross-linked with zirconium (IV)	Phosphate ions	q_{max} = 65.35 mg/g at pH=7 and 293K	[47]
17	Chitosan/bentonite	Cross-linked	Copper (II) ions	% removal =29	[48]
18	Chitosan/bentonite	Ionic exchange by intercalation	Cadmium Ions	q_{max} = 168.7 mg/g at 297K	[49]
19	Chitosan/lanhanu/ bentonite	Ionic exchange by intercalation	Phosphorus ions	% removal=93.2	[50]
20	Chitosan/calcium alginate/bentonite	Ionic exchange by intercalation	Lead ions	q_{max} = 434.89 mg/g	[51]
			Copper ions	q_{max} = 168.7 mg/g	
			Cadmium ions	q_{max} = 168.7 mg/g	

The success of any adsorption process largely depends on the nature, adsorption capacity of the adsorbent used and the optimum process variables. Against this backdrop, the appropriate optimization and modeling tools must be employed to achieve optimum variables conditions for high efficiency removal of the selected PAHs (such as naphthalene used in this study) and the pollutants under consideration. Several modeling tools are in vogue and are widely applied for input-output set of data particularly in engineering fields. Amongst the tools with outstanding performance are response surface methodology (RSM) and adaptive neuro–fuzzy inference logic system (ANFILS). The RSM is considered to be a veritable and versatile mathematical tool for modeling and optimizing experimental data by way of establishing relationship between the single/multiple responses to the several numbers of independent variables [29]. It is a collection of mathematical and statistical techniques for developing empirical models within the confine of second order quadratic equation [52–53]. The benefits of using RSM for modelling and optimization studies include: (i) it allows for a reduced number of experimental trials vis-à-vis the conventional method of one factor at a time; (ii) it integrates mathematical modeling and experimental design; (iii) it possesses the ability to analyze the interaction of process variables with

visual elucidation in spite of the inherent complexity; (iv) it has the capacity of high reasonable optimization degree and (v) it exists in varieties of classes such as Box-Behnken design (BBD), central composite design (CCD), hybrid design, three-level factorial design among others, that suit specific demands [54–55]. To improve the performance of RSM in achieving global optimization, the evolutionary algorithm such as the genetic algorithm, one of the choicest and most popular algorithms, is employed [56]. The adaptive neuro-fuzzy inference logic system or adaptive network-based fuzzy inference logic system (ANFILS) is a part of artificial intelligence (AI) algorithms that map input to output data with high precision accuracy. ANFILS is a hybrid algorithm that blends the pros of artificial neural network (ANN) with the fuzzy logic system [57]. Tanhaei et al. [18] described ANFILS as the model best in data prediction with very low error value. It is commonly used in production and other segment of industries [58–62]; agricultural processes [63] and separation processes for water treatment and purification [18, 19, 64–67]. The dearth of insightful information on the response surface methodology (RSM), RSM–genetic algorithm (GA) and adaptive neuro–fuzzy inference logic system (ANFILS) modeling and optimization of the process variables involved in the adsorption of naphthalene adsorption on chitosan–CTAB–bentonite matrix necessitated this study, which, to the best of our knowledge, has not been reported in the literature. Hence, the primary design of this study is to carry out comparative studies of RSM, RSM–GA and ANFILS for modeling and optimization of naphthalene adsorption on chitosan–CTAB–bentonite matrix. This is with the objectives of obtaining applicable models and optimum conditions for the % removal of naphthalene and adsorption capacity of the synthesized composite adsorbent: ANFILS was adjudged the best to predict these conditions.. The methods of preparation of the adsorbent and its physicochemical properties and characterization were succinctly reported in our previous study [68].

2. Materials and Methods

2.1. Materials

The materials utilized in this study include raw bentonite clay, *Archachatina marginata* (African giant snail) shell wastes, naphthalene in granulated state (C_8H_{10}; mol. wt. = 128.1705 g/mol; purity: >97%); ammonium ethanoate in aqueous form ($CH_3CO_2NH_4$; mol. wt. = 77.08 g/mol; purity: 98%), sodium carbonate in granulated form (Na_2CO_3; mol. wt. = 105.99 g/mol; purity: 98%), sodium hydroxide in pellet form (NaOH; mol. wt. = 40 g/mol; purity: 98%) and cetyltrimethylammonium bromide in granulated form (CTAB) ($[(C_{16}H_{33})N(CH_3)_3]Br$; mol. wt. = 128.1705 g/mol; purity: > 96%) were purchased from Merck, India. Ethanol acid (C_2H_5OH; Absolute 98%) was supplied from BDH laboratories, England while methylene blue in granulated form ($C_{16}H_{18}CIN_3S$; mol. wt. = 319.85 g/mol; Purity: > 97%) was purchased from Loba Chemie, PVT limited India.

2.2. Preparation of composite nanoparticles

The preparation of composite nanoparticles of chitosan–CTAB–Na bentonite clay was outlined in detail in our recent work [68]. The analysis of the raw bentonite clay revealed it to be calcium-bentonite clay, which was modified to obtain sodium-bentonite clay.

2.3. Measurement of the Physicochemical Properties

The physicochemical properties of the resulting chitosan–CTAB–Na bentonite clay nanoparticles determined and reported in our previous study [68] included iodine number, porosity, specific gravity, void volume, moisture content, Hausner ratio, particle density, bulk and tapped density, surface zero-point charge, swelling index, Barrett, Joyner and Halenda (BJH) pore diameter, cation exchange capacity (CEC), total pore volume and micropore volume, which were determined using simple basic laboratory apparatus such as beakers, conical flasks and whatnot.

2.4. Characterization of Chitosan-CTAB-Na Bentonite Clay Hybrid Matrix

The characterization of the prepared chitosan–CTAB–Na bentonite clay nanoparticles, which was reported elsewhere [67], included scanning electron microscopy (SEM), Energy Dispersive X-ray Spectroscopy (EDX) analyzed using JOEL-JSM 7600F model equipment mounted with electron dispersive spectrometer, Brunauer-Emmet-Teller (BET) surface area facilitated with ASAP 2020 V4.02 model, micromeritics instrument corp., USA. The Fourier Transform Infrared Spectroscopy (FTIR) was carried out with Nicolet IS10 model, Thermo Fisher Scientific, Korea Co., Ltd; X–ray fluorescence spectrophotometry analysis was carried out to ascertain the elemental compositions of the constituents and hybrid adsorbent aided by a device (TEFA ORTEC automatic X-ray F 1610, Maharashtra, India) and X-ray Diffraction (XRD) analyses were performed with Rigaku D/Max-111C X-ray diffractometer.

2.5. Experimental naphthalene adsorption study

The experimental adsorption of naphthalene batchwise was detailed in our recent work [68] where the equilibrium amount of naphthalene in the adsorbed phase, q_e mg/g, and the % removal of naphthalene, R_e, using the synthesized composite adsorbent were calculated using Equations (1) and (2) respectively:

$$q_e = \left(\frac{c_0 - c_e}{M_c} \right) V_s \tag{1}$$

$$R_e = \left(1 - c_e / c_0\right) \times 100 \tag{2}$$

where c_e and c_0 are the equilibrium and initial concentrations of naphthalene in the aqueous solution (mg/L), M_c the mass of the composite nanoparticles of chitosan–CTAB–sodium bentonite clay used as adsorbent (g) and V_s the volume of aqueous solution in contact with the adsorbent (L).

3. Optimization studies

Response surface methodology (RSM), hybrid of RSM–genetic algorithm (RSM–GA) and adaptive neural fuzzy inference logic system (ANFILS) are used to model and optimize the synthesis process variables in this study.

3.1. Response surface methodology (RSM)

The response surface methodology (RSM) is a resourceful technique that involves a collection of statistical techniques suitable for analyzing the intricacies of experimental design and model formulation with a view to ascertaining optimum conditions thereby predicting the effects of the process variables on

the response variable [55, 69]. Hence, the behavior and pattern of the composite nanoparticles of chitosan–CTAB–sodium bentonite clay can be modeled by RSM by applying Equation (3) [55]:

$$Y = \Phi_0 + \sum_{i=1}^{k} \Phi_i X_i + \sum_{i=1}^{k} \sum_{j=1}^{k} \Phi_{ij} X_i X_j + \sum_{i=1}^{k} \Phi_{ii} X_{ii}^2 + \in \quad (3)$$

where Y represents the dependent variables, i.e., the responses, Φ_0 , Φ_i , Φ_{ij} , Φ_{ii} are the respective coefficients for constant, linear, interaction and quadratic effects respectively, X_i and X_j are the design factors, i.e., the independent variables.

3.2. Design of Experiment

The central composite design (CCD) of the RSM was used in this work. For a thorough CCD, the number of runs, *N*, is calculated using Equation (4) [70, 71]:

$$N = 2^n + 2n + n_{cr} \quad (4)$$

where the number of factorial runs $\left(= 2^n\right)$, the number of axial runs $\left(= 2n\right)$ to enable the estimation of experimental error, n_{cr} the number of center runs needed to ensure constant variance in model prediction and *n* the number of the independent variables. For four design factors investigated in this study (i.e., concentration of surfactant, time of activation, temperature of activation and dosage of chitosan), the complete experimental design consists of 31 experimental runs with 16, 8 and 7 factorial, axial and center points respectively, which was obtained using Equation (4). Table 2 depicts the values of the coded and uncoded independent variables, experimental range and levels.

Table 2. Coded and uncoded factors for the design of experimental range and levels

Control factors	$-\alpha(-2)$	**-1**	**0**	**1**	$+\alpha(+2)$
Surfactant concentration, X_1, (mg/L)	20	40	60	80	100
Activation time, X_2, (h)	1	1.5	2	2.5	3
Activation temperature, X_3, (°C)	60	70	80	90	100
Chitosan dosage, X_4, (g)	2	3	4	5	6

The coded values were obtained using Equation (5) [72-73]:

$$X_i = \frac{2\left[2X - \left(X_{max} + X_{min}\right)\right]}{X_{max} - X_{min}} \quad (5)$$

where X_i is the required coded value of any variable *X*, whose value ranges from the lower level, X_{min}, of the variable to the upper level, X_{max}, of the variable. The full experimental design is shown in Table 3.

Table 3. Experimental design generated by MINITAB 17

Experimental runs (standard order)	X_1 (mg/L)	X_2 (h)	X_3 (ºC)	X_4 (g)
1	40	1.5	70	3
2	80	1.5	70	3
3	40	2.5	70	3
4	80	2.5	70	3
5	40	1.5	90	3
6	80	1.5	90	3
7	40	2.5	90	3
8	80	2.5	90	3
9	40	1.5	70	5
10	80	1.5	70	5
11	40	2.5	70	5
12	80	2.5	70	5
13	40	1.5	90	5
14	80	1.5	90	5
15	40	2.5	90	5
16	80	2.5	90	5
17	20	2.0	80	4
18	100	2.0	80	4
19	60	1.0	80	4
20	60	3.0	80	4
21	60	2.0	60	4
22	60	2.0	100	4
23	60	2.0	80	2
24	60	2.0	80	6
25	60	2.0	80	4
26	60	2.0	80	4
27	60	2.0	80	4
28	60	2.0	80	4
29	60	2.0	80	4
30	60	2.0	80	4
31	60	2.0	80	4

3.3. Adaptive Neuro-Fuzzy Inference Logic System (ANFILS)

The Adaptive Neuro-Fuzzy Inference Logic System (ANFILS) is a blend of artificial neural network and Takagi-Sugeno type of inference fuzzy system [74]. It is a unique intelligent technique tool for modeling and optimizing simple and complex systems by employing fuzzy rules to describe the system. The literature is replete with facts that the model is fast with accurate learning ability, easy to implement and apply, void of much prior human expertise and accommodate the use of linguistic and numeric knowledge in proffering reasonable desired modeling results with the use of varieties neurons known as membership functions [75, 76]. Detailed information can be obtained in other studies [77–79].

A generalized type–1 TSK model can be described by fuzzy IF–THEN rules, which establishes the input and output relations of any system. The kth rule can be expressed as:

IF x_1 is Q_1^k, x_2 is Q_2^k . . . . . x_n is Q_n^k

THEN y is

$$w^k = f^k(x_1, x_2, \ldots\ldots, x_n) = p_0^k + p_1^k x_1 + p_2^k x_2 + \ldots\ldots + p_n^k x_n \quad (6)$$

where $x_1, x_2, \ldots\ldots, x_n$ are input variables, $Q_1^k, Q_2^k, \ldots\ldots, Q_n^k$ are type of fuzzy sets on $x_1, x_2, \ldots\ldots, x_n$ of any membership function such as gaussian curve (gaussmf), gaussian combination (gauss2mf), π-shaped (pimf), difference between two sigmoidal (dsigmf), product of two sigmoidal (psigmf), triangular shaped (trimf), trapezoidal shaped (trapmf), generalized bell shaped (gbellmf) [80], y is either a constant or a linear function of the input variables and $p_0^k, p_1^k, \ldots\ldots, p_n^k$ are constant regression parameters or linear parameters of consequent part of the kth rule. ANFILS is described by 5 layers feed forward neural network as shown in Figure 1 [81].

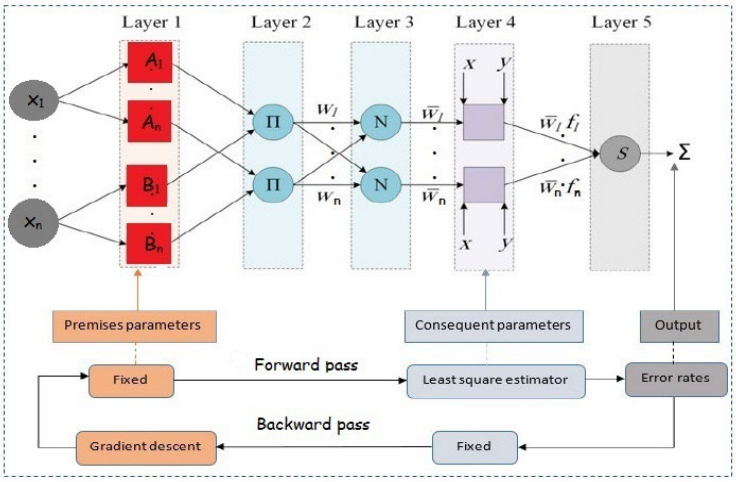

Figure 1. ANFILS architecture and basic principles of operation [82].

Layer 1: This layer is called the input layer. Input variables, $x_1, x_2, \ldots\ldots, x_n$, are passed to the number of neurons to the next layer.

Layer 2: This is called the fuzzification layer. Fuzzification is the commencement of the Fuzzy Inference System (FIS). It is basically where the system takes a real scalar number (otherwise called crisp value) and is converted into a fuzzy linguistic value defined by membership functions [83]. The

layer includes the input variables membership functions (MFs) and each node in this layer is an adaptive node given as:

$$O_1 = \mu_i^k(x_n) \tag{7}$$

where μ_i^k are the many membership functions, i is the membership grade of the fuzzy sets $(A_1, A_2, \ldots\ldots, A_n, B_1, B_2, \ldots\ldots, B_n)$ and O_1 is the output of the node i. In this present work, the membership function applied is the bell-shaped type given as:

$$\mu_i^k(x_n) = \frac{1}{1+\left(\frac{x-c}{a}\right)^{ab}} \tag{8}$$

This function contains three parameters a, b and c with each having values ranging between the lowest and highest amount of 0 and 1 [84].

Layer 3: This is referred as the implication layer where the firing strength of a rule is ascertained by product operation ($\cap$) such that:

$$O_2 = w_i = \mu_1^k(x_1) \cap \mu_2^k(x_2) \cap \ldots\ldots \cap \mu_n^k(x_n) \tag{9}$$

Layer 4: This layer is called the normalization layer where the normalization firing strength or weights of rules are evaluated thus:

$$O_3 = \overline{w}_i = \frac{w_i}{w_i + \ldots + w_n}, \; i = 1, 2, \ldots\ldots, n \tag{10}$$

Layer 5: This layer is the defuzzification layer and the nodes are adaptive with node function. This layer paves way for the output results from the inference of rules employed.

$$O_i^4 = \overline{w}_i y_i, \; i = 1, 2, \ldots\ldots, n \tag{11}$$

This is the output layer with non-adaptive node where all the results from the previous layer all summed up as expressed in Equation (12):

$$O_5 = \overline{w}_i f^k(x_1, x_2, \ldots\ldots, x_n) = \overline{w}_i \left(p_0^k + p_1^k x_1 + p_2^k x_2 + \ldots\ldots + p_n^k x_n\right) \tag{12}$$

It transforms the fuzzy classification results into a crisp or binary number.

The data points are segmented into 2 parts, training and testing sets, and normalized using the expression [85]:

$$x_n = \frac{x - x_{min}}{x_{max} - x_{min}} \tag{13}$$

where x and x_n are measured and normalized values respectively, x_{max} and x_{min} denote the maximum and minimum values of x respectively. The training ensures the creation of the ANFILS architecture structure while the testing sets validate the prediction accuracy of the model. 80% of the data sets were used for training process while 20% were applied for testing. The learning or training process is tailored towards tunning the premise and consequent parameter sets to map the desired output using the least square estimation (LES) and gradient descent (GD) method in a forward and backward mode. The former entails keeping the premise parameters fixed while the consequent parameters are varied until optimal values. The latter employs the use of gradient descent (GD) with back propagation techniques from the output layer to the input layer [86]. Khoshnevisan et al. [84] listed the following as factors for achieving a least error network:

(i) the number of membership function;
(ii) types of output functions in terms of constant or linear;
(iii) optimization method adopted, which could be hybrid or back propagation; and
(iv) number of epochs or training carried out.

Figure 2 shows the ANFILS architecture characterized with 4 inputs, 3 membership functions and 81 fuzzy rules.

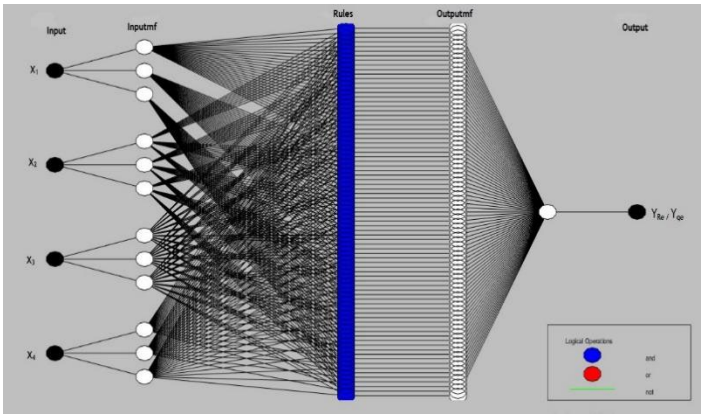

Figure 2. ANFILS architecture for input and output data.

3.4. Error functions

The following error functions are used to compare the RSM and ANFILS models' adequacy in predicting the experimental adsorption data of naphthalene on the synthesized chitosan–CTAB–Na bentonite clay matrix [87, 88–90]:

$$R^2 = 1 - \frac{\sum_{i=1}^{n}\left(\varphi_{i,e} - \varphi_{i,p}\right)^2}{\sum_{i=1}^{n}\left(\varphi_{i,p} - \varphi_{e}\right)^2} \tag{14}$$

$$adj.R^2 = 1 - \left[\left(1 - R^2\right) \times \frac{n-1}{n-k-1}\right] \tag{15}$$

$$RMSE = \sqrt{\frac{\sum_{i=1}^{n}\left(\varphi_{i,p} - \varphi_{i,e}\right)^2}{n}} \tag{16}$$

$$MAE = \frac{1}{n}\sum_{i=1}^{n}\left|\varphi_{i,e} - \varphi_{i,p}\right| \tag{17}$$

$$MAPE = \frac{1}{n}\sum_{i=1}^{n}\left(\frac{\varphi_{i,e} - \varphi_{i,p}}{\varphi_{i,e}}\right) \tag{18}$$

$$MPE = \frac{100}{n}\sum_{i=1}^{n}\left|\frac{\varphi_{i,e} - \varphi_{i,p}}{\varphi_{i,p}}\right| \tag{19}$$

$$SEP = \left(RMSE/\varphi_e\right)\times 100 \tag{20}$$

$$TIC = \frac{\sqrt{\frac{1}{n}\sum_{i=1}^{n}\left(\varphi_{i,p} - \varphi_{i,e}\right)^2}}{\sqrt{\frac{1}{n}\sum_{i=1}^{n}\varphi_{i,e}^2} + \sqrt{\frac{1}{n}\sum_{i=1}^{n}\varphi_{i,p}^2}} \tag{21}$$

$$WI = 1 - \frac{\sum_{i=1}^{n}\left(\varphi_{i,e} - \varphi_{i,p}\right)^2}{\sum_{i=1}^{n}\left[\left|\varphi_{i,p} - \overline{\varphi}_p\right| + \left|\varphi_{i,e} - \overline{\varphi}_e\right|\right]^2}, \quad 0 \le WI \le 1 \tag{22}$$

$$R = \frac{\sum_{i=1}^{n}\left(\left|\varphi_{i,e} - \overline{\varphi}_e\right|\right)\left(\left|\varphi_{i,p} - \overline{\varphi}_p\right|\right)}{\sqrt{\sum_{i=1}^{n}\left(\varphi_{i,e} - \overline{\varphi}_e\right)^2}\sqrt{\sum_{i=1}^{n}\left(\varphi_{i,p} - \overline{\varphi}_p\right)^2}} \tag{23}$$

$$CI = WI \times R \tag{24}$$

where n is the number of experimental runs, $\varphi_{i,e}$ [$= \left(R_e\right)_{i,e\,xpt}$ or $\left(q_e\right)_{i,e\,xpt}$] the measured adsorption data for run i, $\varphi_{i,p}$ [$= \left(R_e\right)_{i,pred}$ or $\left(q_e\right)_{i,pred}$] the predicted (or calculated) adsorption data for run i, $\overline{\varphi}_e$ and $\overline{\varphi}_p$ the mean of the experimental and predicted adsorption data respectively, R^2 is the coefficient of determination, *RMSE* the root mean square, *MAE* the mean absolute error, *MAPE* the mean absolute percentage error, *MPE* the mean percentage error, *SPE* the standard error prediction, *TIC* the Theil Inequality Coefficient, *WI* the Willmott index and *CI* the confidence or performance index.

The fit of the predicted % removal of naphthalene and adsorption capacity of the chitosan–CTAB–Na bentonite matrix as adsorbent with the experimental data can equally be developed based on the statistical function such as the Durbin-Watson Test (DWT). The DWT is an autocorrelation test in the differences between the experimental and predicted data (i.e., the residuals) from the analysis of statistical regression, such that $0 \le DWT \le 4$. For positive and negative autocorrelations,

$0 \le DWT < 2$ and $2 < DWT \le 4$ respectively. However, there is no autocorrelation detected in the sample if $DWT = 2.0$. The value of *DWT* must be at least 1.0 for a good model [91]. The Durbin-Watson statistic is given by Olafadehan [88]:

$$DWT = SDS/SES \tag{25}$$

where the sum of errors squared, *SES,* is given by:

$$SES = \sum_{i=1}^{n} \left(\varphi_{i,e} - \varphi_{i,p}\right)^2 = \varepsilon_1^2 + \varepsilon_2^2 + \varepsilon_3^2 + \ldots + \varepsilon_{n-1}^2 + \varepsilon_n^2 \tag{26}$$

and the sum of differences squared (*SDS*) is given by:

$$SDS = \left(\varepsilon_2 - \varepsilon_1\right)^2 + \left(\varepsilon_3 - \varepsilon_2\right)^2 + \left(\varepsilon_4 - \varepsilon_3\right)^2 + \ldots + \left(\varepsilon_n - \varepsilon_{n-1}\right)^2 \tag{27}$$

and ε_i $(i = 1, 2, \ldots, n)$ is the difference between the experimental adsorption data, $\varphi_{i,e}$ and the predicted value, $\varphi_{i,p}$.

4. Results and Discussion

4.1. Characterization of the chitosan-CTAB-Na bentonite clay nanoparticles

The physicochemical characteristics of the composite nanoparticles of chitosan–CTAB–sodium bentonite clay used as adsorbent in this study was reported elsewhere [68].

4.2. RSM analysis

With the application of multiple regression analysis and stepwise optimization option via MINITAB 17 software, while maintaining the hierarchical structure, the resulting second-order quadratic equation of the operating variables on the response variables is given in uncoded unit as:

$$Y_{R_e} = -38.7 + 0.930X_1 + 41.4X_2 + 1.279X_3 + 11.46X_4 - 0.00301X_1^2 - 13.37X_2^2 - 0.00728X_3^2 - 0.915X_4^2 - 0.217X_1X_2 - 0.0468X_1X_4 \tag{28}$$

$$Y_{q_e} = -96.9 + 2.324X_1 + 103.5X_2 + 3.20X_3 + 28.7X_4 - 0.00754X_1^2 - 33.4X_2^2 - 0.0182X_3^2 - 2.29X_4^2 - 0.542X_1X_2 - 0.1170X_1X_4 \tag{29}$$

where Y_{R_e} is the percentage removal of naphthalene and Y_{q_e} the adsorption capacity of the composite adsorbent. The process variables, X_1, X_2, X_3 and X_4 are the concentration of surfactant, time of activation, temperature of activation and dosage of chitosan respectively.

The fitness of the model equation was evaluated using the coefficient of determination, R^2. Tables 4 and 5 show the results of the ANOVA response surface quadratic models for percentage removal of naphthalene and the adsorption capacity of the synthesized composite nanoparticles of chitosan–CTAB–sodium bentonite clay. In these tables, there is need to emphasize that when RSM technique is employed with the use of MINITAB before the generation of model equation and ANOVA analysis by the software,

options such as, “stepwise”, “forward” and “backward” are provided to eliminate some of the non-significant terms and while others are retained to maintain hierarchical model equation. X_1X_3, X_1X_4 and X_2X_3 were part of the non-significant terms that were eliminated while X_1X_2 and X_1X_4 were the only two terms retained when the stepwise option was chosen, as revealed in Equations (28) and (29).

Table 4. ANOVA response surface quadratic model summary for percentage removal of naphthalene on chitosan–CTAB–sodium bentonite clay matrix

Standard deviation	R^2	**adj.** R^2	**pred.** R^2
2.4247	86.39%	79.59%	54.24%

Term	Effect	Coded coefficient	SE coefficient	*t*-value	*p*-value	VIF
Constant		95.663	0.916	104.39	0.000	
X_1	8.736	4.368	0.495	8.83	0.000	1.00
X_2	4.168	2.084	0.495	4.21	0.000	1.00
X_3	2.278	1.139	0.495	2.30	0.032	1.00
X_4	2.676	1.338	0.495	2.70	0.014	1.00
X_1^2	-2.412	-1.206	0.453	-2.66	0.015	1.03
X_2^2	-1.672	-0.836	0.453	-1.84	0.080	1.03
X_3^2	-1.457	-0.728	0.453	-1.61	0.124	1.03
X_4^2	-1.829	-0.915	0.453	-2.02	0.057	1.03
X_1X_2	-2.166	-1.083	0.606	-1.79	0.089	1.00
X_1X_4	-1.871	-0.936	0.606	-1.54	0.138	1.00

Table 5. ANOVA response surface quadratic model summary for adsorption capacity of chitosan–CTAB–sodium bentonite clay matrix

Standard deviation	R^2	**adj.** R^2	**pred.** R^2
6.06167	86.39%	79.59%	54.24%

Term	Effect	Coded coefficient	SE coefficient	*t*-value	*p*-value	VIF
Constant		239.16	2.29	104.39	0.000	
X_1	21.84	10.92	1.24	8.83	0.000	1.00
X_2	10.42	5.21	1.24	4.21	0.000	1.00
X_3	5.69	2.85	1.24	2.30	0.032	1.00
X_4	6.69	3.34	1.24	2.70	0.014	1.00
X_1^2	-6.03	-3.01	1.13	-2.66	0.015	1.03
X_2^2	-4.18	-2.09	1.13	-1.84	0.080	1.03
X_3^2	-3.64	-1.82	1.13	-1.61	0.124	1.03

X_4^2	-4.57	-2.29	1.13	-2.02	0.057	1.03
X_1X_2	-5.42	-2.71	1.52	-1.79	0.089	1.00
X_1X_4	-4.68	-2.34	1.52	-1.54	0.138	1.00

From Tables 4 and 5, the regression coefficient of the developed models, Equations (28) and (29), and the adjusted regression coefficient, *adj.* R^2, are the same as 86.39% and 79.59% respectively. This implies that 13.61% of the total variations were not adequately explained by the model equations.

The Fischer's "F–statistical" (or *F*–test) was employed to determine the statistical significance of the model. It facilitates the evaluation of the quality of prediction by the model when all design factors are considered at a time [92]. The comments on the ANOVA for response surface quadratic models for percentage removal of naphthalene and adsorption capacity of the composite nanoparticles of chitosan–CTAB–sodium bentonite clay are provided in Tables 6 and 7.

Table 6. Comment on the ANOVA for response surface quadratic model for percentage removal of naphthalene on chitosan–CTAB–sodium bentonite clay matrix

Source	**DF**	**Adj. SS**	**Adj. MS**	**F-value**	**p-value**	**Comment**
Model	10	746.55	74.655	12.70	0.000	Significant
Linear	4	636.18	159.045	27.05	0.000	Significant
X_1	1	457.89	457.889	77.89	0.000	Significant
X_2	1	104.21	104.208	17.73	0.000	Significant
X_3	1	31.12	31.122	5.29	0.032	Significant
X_4	1	42.96	42.961	7.31	0.014	Significant
Square	4	77.59	19.397	3.30	0.031	Significant
X_1^2	1	41.58	41.578	7.07	0.015	Significant
X_2^2	1	19.98	19.977	3.40	0.080	Not Significant
X_3^2	1	15.17	15.169	2.58	0.124	Not Significant
X_4^2	1	23.92	23.918	4.07	0.057	Not Significant
2-way interaction	2	32.78	16.388	2.79	0.086	Not Significant
X_1X_2	1	18.77	18.771	3.19	0.089	Not Significant
X_1X_4	1	14.01	14.006	2.38	0.138	Not Significant
Error	20	117.58	5.879			
Lack-of-Fit	14	105.44	7.532	3.72	0.057	Significant
Pure Error	6	12.14	2.023			
Total	30	864.13				

Table 7. Comment on the ANOVA for response surface quadratic model of the adsorption capacity of chitosan–CTAB–Na bentonite clay matrix

Source	DF	Adj. SS	Adj. MS	F-value	p- value	Comment
Model	10	4665.91	466.59	12.70	0.000	Significant
Linear	4	3976.12	994.03	27.05	0.000	Significant
X_1	1	2861.80	2861.80	77.89	0.000	Significant
X_2	1	651.30	651.30	17.73	0.000	Significant
X_3	1	194.51	194.51	5.29	0.032	Significant
X_4	1	268.50	268.50	7.31	0.014	Significant
Square	4	484.93	121.23	3.30	0.031	Significant
X_1^2	1	259.86	259.86	7.07	0.015	Significant
X_2^2	1	124.85	124.85	3.40	0.080	Not Significant
X_3^2	1	94.80	94.80	2.58	0.124	Not Significant
X_4^2	1	149.49	149.49	4.07	0.057	Not Significant
2-way Interaction	2	204.86	102. 43	2.79	0.086	Not Significant
X_1X_2	1	117.32	117.32	3.19	0.089	Not Significant
X_1X_4	1	87.54	87.54	2.38	0.138	Not Significant
Error	20	734.88	36.74			
Lack-of-Fit	14	659.03	47.07	3.72	0.057	Significant
Pure Error	6	75.85	12.64			
Total	30	5400.79				

From Tables 6 and 7, a high value of the Fischer's "F–statistical" value of 12.70 (the ratio of the mean square due to regression to the mean square due to residual error) with low probability, *p*, of 0.000 indicates high reliability and significance of the model equations. The response variables *p*-value of 0.057 for the lack of fit implies that it is not significant and any presumed negative influence on the accuracy of the model should be jettisoned [93]. The significance of the models' terms was verified based on individual *p* values. The results in Tables 4–7 show similar results where the single terms, X_1, X_2, X_3 and X_4 are statistically significant since $p<0.05$ at 95% confidence level interval. For the square terms, only the surfactant concentration, X_1^2, is the statistically significant term while others were statistically insignificant. The interactive terms, X_1X_2 and X_1X_4, were statistically insignificant by virtue of their corresponding p values being greater than 0.05. The significance of the regression coefficient was examined by the student's *t*–test. The coefficient with larger *t* value and corresponding low value of *p* indicates high significance. Also, the negative and positive signs depict the effect of antagonism and synergism respectively on the response variables [55, 94]. All the single terms have synergistic effect on the response variables while the square terms and interactive terms have antagonistic effect on the response variables. To ascertain the effect in terms of percentage, the Pareto analysis was employed, based on Equation (30) [85, 95]:

$$P_i=\left(B_i^2/\sum B_i^2\right)\times 100 \quad (i=0) \tag{30}$$

where P_i is the Pareto percentage importance of variables and B_i^2 the regression coefficient of each process variables.

The surfactant concentration, X_1, time of activation, X_2, chitosan dosage, X_4, surfactant concentration square term, X_1^2, temperature of activation, X_3, interactive term of surfactant concentration and time of activation, X_1X_2, square term of chitosan dosage, X_4^2, interactive term of surfactant concentration and chitosan dosage, X_1X_4, square term of time of activation, X_2^2 and square term of temperature of activation, X_3^2, followed accordingly in line of their degrees of effect on the response variables, as shown in Table 8.

Table 8. Pareto analysis of percentage effect of regression coefficients on the model equation

Variable	Percentage importance of regression coefficient for % removal	Percentage importance of regression coefficient for adsorption capacity	Ranking
X_1	59.4774	59.4789	1
X_2	13.5389	13.5392	2
X_3	4.0442	4.0372	5
X_4	5.5808	5.5810	3
X_1^2	4.5340	4.5341	4
X_2^2	2.1787	2.1788	9
X_3^2	1.6544	1.6522	10
X_4^2	2.6071	2.6043	7
X_1X_2	3.6563	3.6632	6
X_1X_4	2.7282	2.7312	8

The two-dimensional (2–D) contour plot and the three-dimensional response (3–D) plot, shown in Figures 3–6, give an insight of the interactive effect of the process variables on the response variables by aiding to achieve the largest percentage removal of naphthalene and adsorption capacity of the adsorbent at the estimated optimum conditions of the process variables for the production of adsorbent. Specifically for the contour plot, a saddle or an elliptical shape gives an impression of the significance of the interactions that exists between the independent (process) variables [93], especially when the model contains a quadratic statistically significant term or it depicts a good correlation between any two independent variables under consideration [86] while others are kept at fixed value usually at the center level. The contour plot in circular form or shape describes negligible interaction [92]. A close observation of the contour plot shows a rising ridge pattern whose response variables increase tremendously as one moves along both axes with darkest and lightest color region located respectively at the upper right and lower left corner of the plot reflecting higher and lower values respectively of the responses variables as the process variables interact.

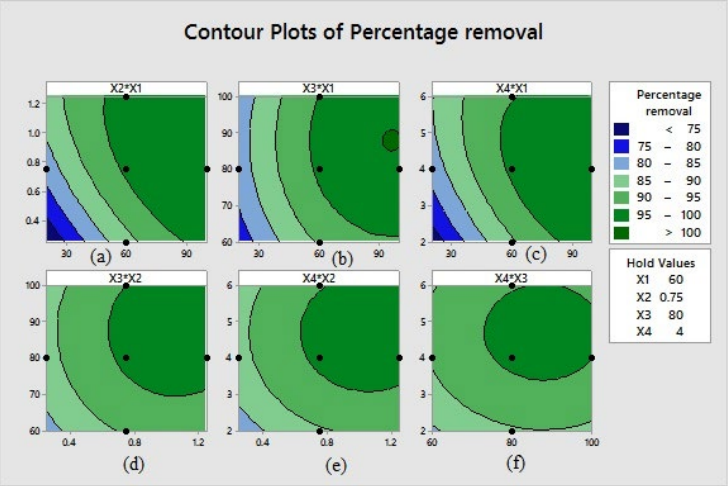

Figure 3. Two-dimensional (contour) plot of percentage removal of naphthalene, (a) interaction of surfactant concentration, X_1, and activation time, X_2, (b) interaction of surfactant concentration, X_1, and activation temperature, X_3, (c) interaction of surfactant concentration, X_1, and chitosan dosage, X_4, (d) interaction of activation time, X_2, and activation temperature, X_3, (e) interaction of activation time, X_2, and chitosan dosage, X_4, and (f) interaction of activation temperature X_3, and chitosan dosage, X_4.

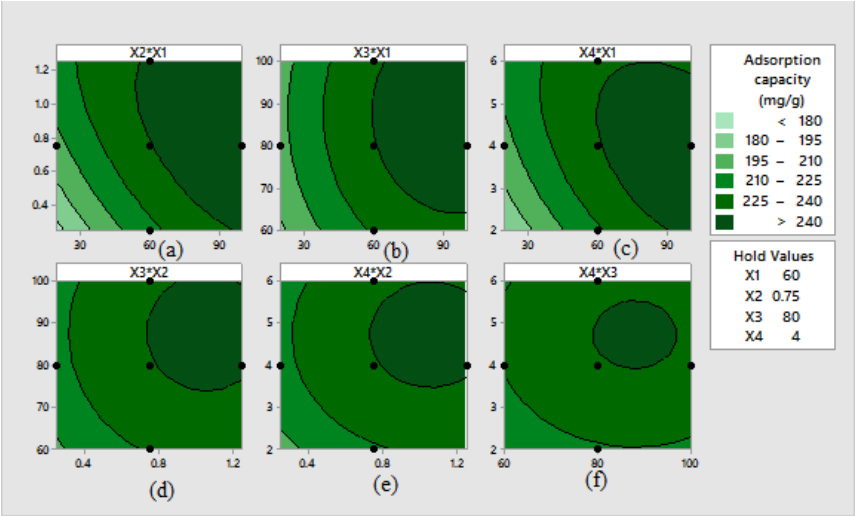

Figure 4. Two-dimensional (contour) plot of adsorption capacity of chitosan–CTAB–Na bentonite clay matrix, (a) interaction of surfactant concentration, X_1, and activation time, X_2, (b) interaction of surfactant concentration, X_1, and activation temperature, X_3, (c) interaction of surfactant concentration, X_1, and chitosan dosage, X_4, (d) interaction of activation time, X_2, and activation temperature, X_3, (e) interaction of activation time, X_2, and chitosan dosage, X_4, and (f) interaction of activation temperature X_3, and chitosan dosage, X_4.

For the 3-D plot, Figures 5 and 6 illustrate a similar trend for all the interactive variables for both response variables. Figures 5(a) and 6(a) show that the percentage of naphthalene removal and adsorption capacity of chitosan–CTAB–Na bentonite clay matrix increase as the interaction of surfactant concentration, X_1, and activation time, X_2, increases. However, both responses increase up to the activation time of 2.5 h before experiencing briefly a plateau and thereafter a slight decrease in the response variables was observed. Figures 5(b) and 6(b) show that the response variables increase as the surfactant concentration, X_1, increases steadily with a corresponding moderate increment in activation temperature, X_3, up to 90°C before recording a slight decrement in the response variables. Figures 5(c) and 6(c) illustrate the combined effects of chitosan dosage, X_4, and surfactant concentration, X_1, on the percentage removal of naphthalene and adsorption capacity of chitosan–CTAB–Na bentonite clay matrix.

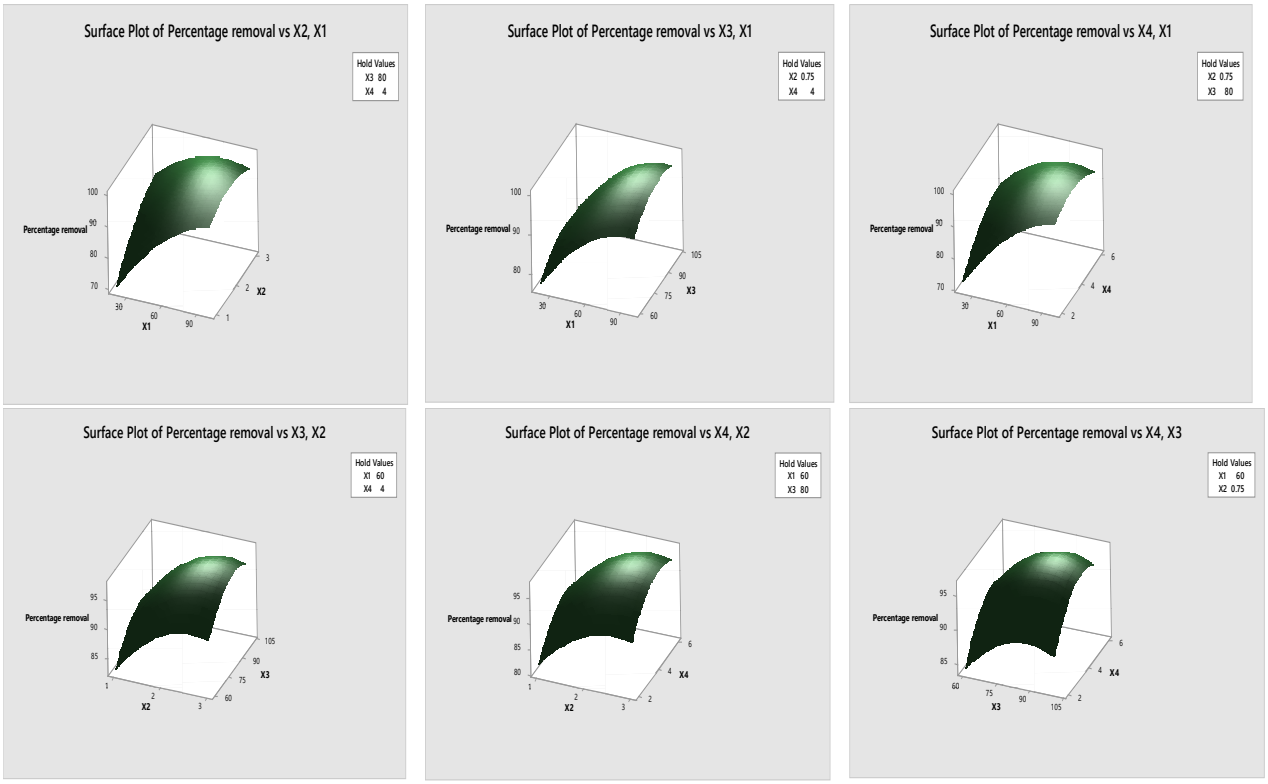

Figure 5. Three-dimensional plot of percentage removal of naphthalene, (a) interaction of surfactant concentration, X_1, and activation time, X_2, (b) interaction of surfactant concentration, X_1, and activation temperature, X_3, (c) interaction of surfactant concentration, X_1, and chitosan dosage, X_4, (d) interaction of activation time, X_2, and activation temperature, X_3, (e) interaction of activation time, X_2, and chitosan dosage, X_4, and (f) interaction of activation temperature X_3, and chitosan dosage, X_4.

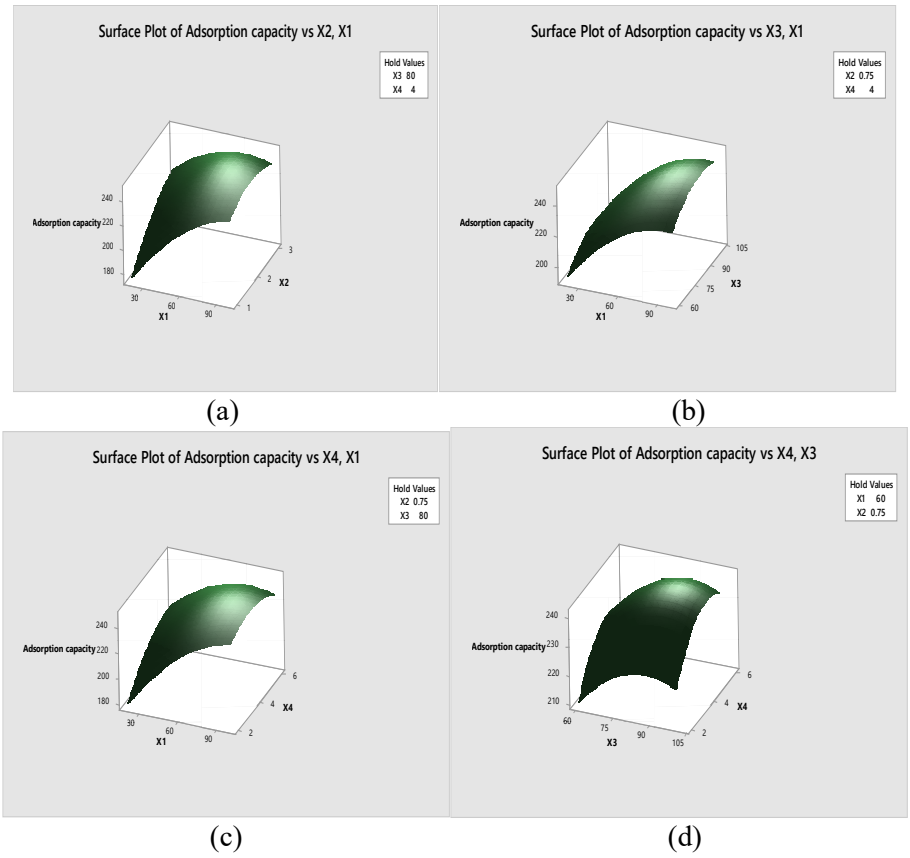

Figure 6. Three-dimensional plot of the adsorption capacity of chitosan–CTAB–Na bentonite clay matrix (a) interaction of surfactant concentration, X_1, and activation time, X_2, (b) interaction of surfactant concentration, X_1, and activation temperature, X_3, (c) interaction of surfactant concentration, X_1, and chitosan dosage, X_4, and (d) interaction of activation temperature, X_3, and chitosan dosage, X_4.

Hence, respective increases in the response variables were observed as surfactant concentration, X_1, increases alongside with chitosan dosage, X_4, up to 80 mg/L and 4 g respectively after which a slight downward progression in the amount of naphthalene removed and the adsorption capacity was observed. Equally, the interaction of activation time, X_2, and activation temperature, X_3, portends increase in the amount of naphthalene removed as the activation temperature increases up to 90°C and activation time of 2.5 h before exhibiting a constant value or non-significant change as illustrated in Figure 5(d). The same trend was observed for the adsorption capacity (though the figure was not presented). In the same vein, the interaction of activation time, X_2, and chitosan dosage, X_4, gives rise to an increase in the percentage amount removed as the values of the process variables increase up to 2.5 h and 5 g respectively before recording slight decrement as depicted in Figure 5(e). The same trend was observed for the adsorption capacity (though the figure was not presented). In a similar development, the collaborative effect of activation temperature, X_3, and chitosan dosage, X_4, shown in Figures 5(f) and

6(d) for the percentage removal of naphthalene and adsorption capacity respectively, signified increase in the response variables as the values of the interacting variables reached 90ºC and 5 g respectively before observing slight downtrends in the % removal of naphthalene and adsorption capacity of chitosan–CTAB–Na bentonite clay matrix.

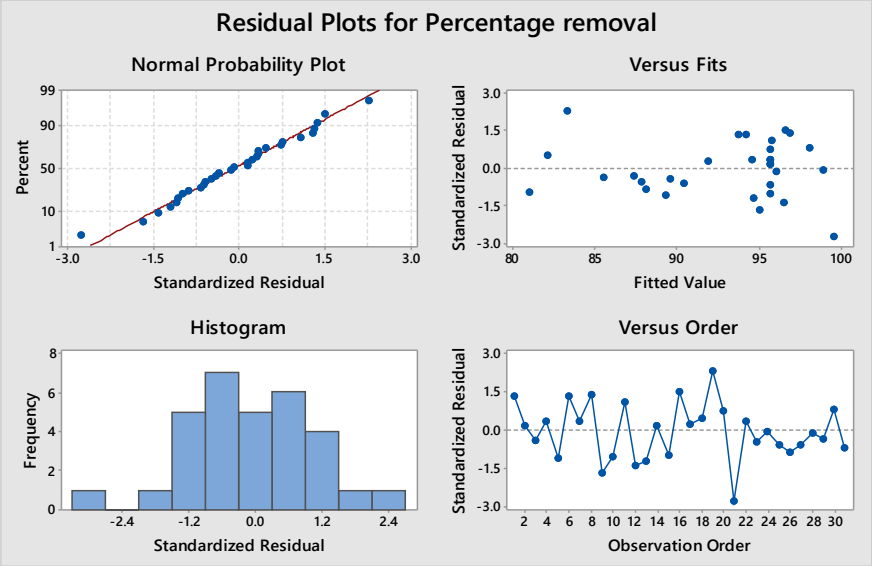

(a)

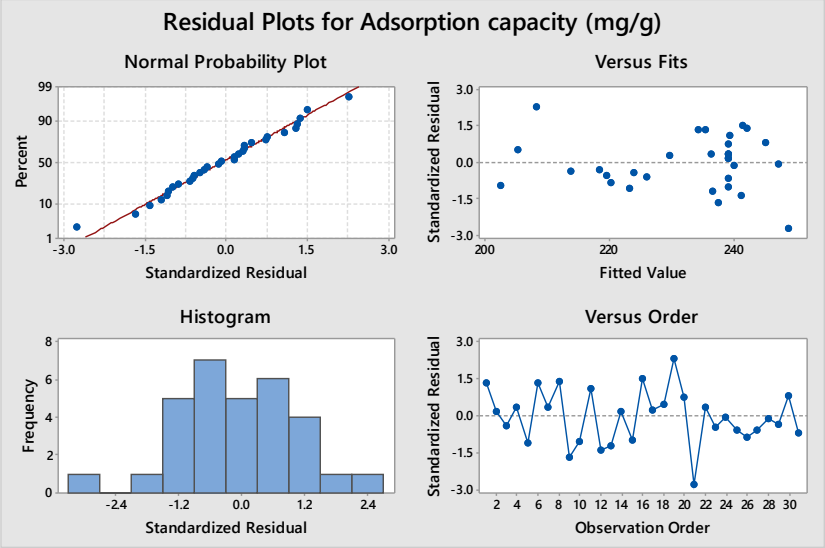

(b)

Figure 7. Residual plots of (a) percentage removal of naphthalene, (b) adsorption capacity of chitosan–CTAB–sodium bentonite matrix clay.

Figures 7(a) and (b) project the residual plots for percentage removal of naphthalene and the adsorption capacity of chitosan–CTAB–sodium bentonite clay matrix respectively. The plots entail the

normal probability plot, standardized residual versus fitted value plot, histogram of standardized residual plot and standardized residual versus observation order plot.

The normal probability plot is used to check for normality of the process variables as it affects the response variables [96]. The distribution proximity of the points around the mean or zero line depicts that the residuals are normally distributed [73, 97–99]. The plots of residuals versus the fitted values for both responses assist to ascertain the sufficiency of the functional part of models while the plots of residual versus order for both responses seek to check for the possible drift or outliers in the process. The distribution proximity of the points around the mean or zero line depicts that the residuals are normally distributed. However, for both responses, minimal divergence of the standardized residuals expectedly was observed, which are projected in the form of "S" shape [97]. The good distributions of residuals in the residuals versus fitted value plots and histogram plots for both responses, and the lack of a specific pattern in the residual versus observation order plots for both responses is a reflection and attestation of the adequacy of the model equation [99–101].

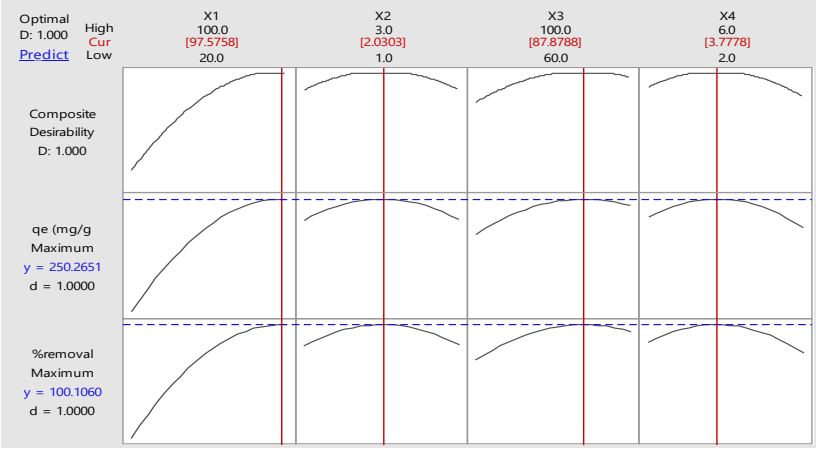

Figure 8. Response optimizer at the optimum condition for the maximum response variables

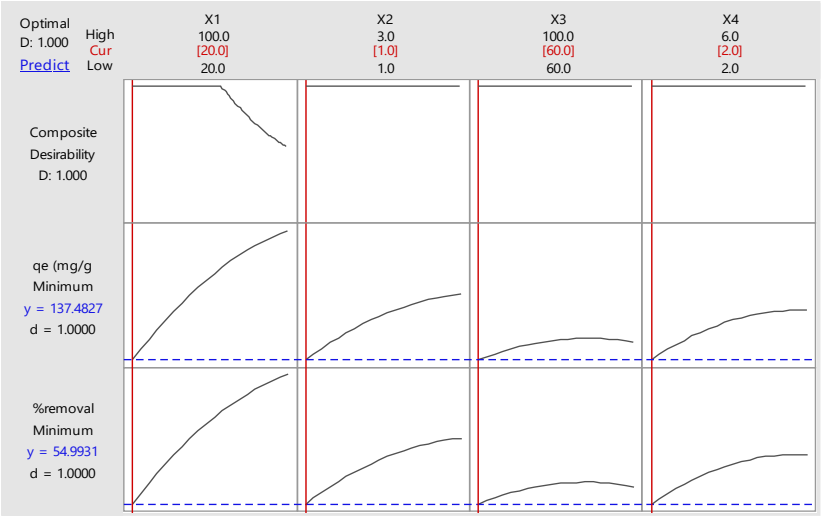

Figure 9. Response optimizer at the optimum condition for the minimum response variables.

The response optimizer was utilized to estimate the best optimum conditions of the process variables. The overall result suggested by MINITAB presumed to be the best, given in red coloration, are shown in Figures 8 and 9 for maximum and minimum response variables (i.e., the percentage removal of naphthalene and adsorption capacity of the chitosan–CTAB–sodium bentonite clay) respectively. The optimum conditions for the maximum response variables were obtained as: surfactant concentration, X_1 = 97.5758 mg/L, activation time, X_2 = 2.03 h, activation temperature, X_3 = 87.88°C and chitosan dosage, X_4 = 3.78 g for maximum response variables while for minimum response variables, the optimum conditions were obtained as: X_1 = 20 mg/L, X_2 = 1 h, X_3 = 60°C and X_4 = 2.0 g.

4.3. Relative importance of process variables

The response model sensitive analysis was used to ascertain the relative importance of the process variables with the aid of *nntool* in MATLAB 2018 software. Table 9 shows the sensitivity analysis of the process values.

Table 9. Sensitivity analysis of process variables

S/No.	Parameters	RMSE	R^2	Best linear equation	Ranking
1	X_1	3.3982	0.5885	Y=0.9465X + 4.8217	1
2	X_2	4.9719	0.1327	Y=0.8963X +8.9953	2
3	X_3	5.1923	0.0451	Y=0.8085X +17.351	4
4	X_4	5.1235	0.0603	Y=1.0583X - 5.164	3
		Double-factor effect			
5	X_1X_2	2.9669	0.6998	Y=0.7869X +19.822	1
6	X_1X_3	3.3777	0.6004	Y=0.8929X +9.7844	3
7	X_1X_4	3.0947	0.6565	Y=1.0069X – 0.5995	2
8	X_2X_3	4.9509	0.1460	Y=0.7062X + 27.296	4
9	X_2X_4	5.6640	0.0875	Y=0.4005X +56.079	5
10	X_3X_4	5.4667	0.0599	Y=0.41X +54.561	6
		Three-factor effect			
11	$X_1X_2X_3$	2.3473	0.8038	Y=0.9979X + 0.398	2
12	$X_1X_2X_4$	2.2922	0.8143	Y=0.8366X +15.555	1
13	$X_2X_3X_4$	5.3133	0.1570	Y=0.4903X + 47.273	3

		Four-factor effect		
14	$X_1X_2X_3X_4$	1.0935	0.9745	Y=0.9628X +3.4044

The results in Table 9 show that surfactant concentration, X_1, exhibits the highest regression value of 0.5885 and *RSME* minimum error of 3.398, amongst the single factors considered, followed by X_2, X_3 and X_4 sequentially. For the double interactive effect, the interaction of surfactant concentration, X_1, and activation time, X_2, has the highest effect with highest regression value (R^2= 0.6998, *RSME* = 2.967) while the interaction of surfactant concentration, X_1, and chitosan dosage, X_4, X_1 and X_3, X_2 and X_3, X_2 and X_4, and X_3 and X_4 ranked second, third, fourth, fifth and sixth respectively. Similarly, the surfactant concentration, X_1, activation time, X_2, and chitosan dosage, X_4, gave the highest effect amongst the three factors (R^2 = 0.8143, *RSME* = 2.2922). Finally, the four factors interaction gave a high regression coefficient (R^2= 0.9745) in predicting the response variables where the value of *RSME* decreased from 2.2922 to 1.0935 with the inclusion of X_3.

4.4. Results using adaptive neuro-fuzzy inference logic system (ANFILS)

The Fuzzy inference system (FIS), membership function and ruler view for input-output relationship and the 1-81 rules of the ANFIS model were then generated while the ANFILS loading training data, loading testing data, training and testing loaded data base on error estimation were considered.

Table 10 shows evidently the effect of the number of membership function, function type, output function and fuzzy inference system optimization method on the error obtained on the training sets and testing sets to achieve the optimal architecture.

Table 10. Effect of the number of membership function; function type, output function and fuzzy inference system optimization method on the error obtained on the training sets and testing sets

S/No.	No. of membership function	Function type	Output function		Training FIS Optimization Method	Error (RMSE) after 100 epochs	
						Training error	Testing error
1	3 3 3 3	Trimf	Linear	Grid portioning	Hybrid	0.0287	0.2488
	15 15 15 15			Cluster categorization	Hybrid	0.0287	0.2177
	3 3 3 3		Constant	Grid portioning	Hybrid	0.0287	0.2875
	15 15 15 15			Cluster categorization	Hybrid	0.0287	0.2177
2	3 3 3 3	Trapmf	Linear	Grid portioning	Hybrid	0.0287	0.2661
	15 15 15 15			Cluster categorization	Hybrid	0.0287	0.2177
	3 3 3 3		Constant	Grid portioning	Hybrid	0.0287	0.2957
	15 15 15 15			Cluster	Hybrid	0.0287	0.2177

				categorization			
3	3 3 3 3 15 15 15 15	Gbellmf	Linear	Grid portioning	Hybrid	0.0287	0.0287
				Cluster categorization	Hybrid	0.0287	0.2177
	3 3 3 3 15 15 15 15		Constant	Grid portioning	Hybrid	0.0287	0.2834
				Cluster categorization	Hybrid	0.0287	0.2177
4	3 3 3 3	gaussmf	Linear	Grid portioning	Hybrid	0.0287	0.2361
				Cluster categorization	Hybrid	0.0287	0.2177
	3 3 3 3 15 15 15 15		Constant	Grid portioning	Hybrid	0.0287	0.2671
				Cluster categorization	Hybrid	0.0287	0.2177
5	3 3 3 3 15 15 15 15	gauss2mf	Linear	Grid portioning	Hybrid	0.0287	0.2465
				Cluster categorization	Hybrid	0.0287	0.2177
	3 3 3 3 15 15 15 15		Constant	Grid portioning	Hybrid	0.0287	0.3017
				Cluster categorization	Hybrid	0.0287	0.2177
6	3 3 3 3 15 15 15 15	pimf	Linear	Grid portioning	Hybrid	0.0287	0.2409
				Cluster categorization	Hybrid	0.0287	0.2177
	3 3 3 3 15 15 15 15		Constant	Grid portioning	Hybrid	0.0287	0.3028
				Cluster categorization	Hybrid	0.0287	0.2177
7	3 3 3 3 15 15 15 15	Dsigmf	Linear	Grid portioning	Hybrid	0.0287	0.2428
				Cluster categorization	Hybrid	0.0287	0.2177
	3 3 3 3 15 15 15 15		Constant	Grid portioning	Hybrid	0.0287	0.3800
				Cluster categorization	Hybrid	0.0287	0.2177
8	3 3 3 3 15 15 15 15	Psigmf	Linear	Grid portioning	Hybrid	0.0287	0.3029
				Cluster categorization	Hybrid	0.0287	0.2177
	3 3 3 3		Constant	Grid portioning	Hybrid	0.0287	0.3801
				Cluster categorization	Hybrid	0.0287	0.2177

From Table 10, the generalized bell-shaped membership function performs better than the other function types owing to the least value of error registered by the training and testing data sets, which lead to the estimation of 36 membership function parameters, 405 consequent parameters and 441 total parameters, which include other settings, as presented in Table 11.

Table 11. ANFILS parameter settings

S/No.	Parameters	Type
1	FIS type	Sugeno
2	MF type	Generalized bell shaped
3	Number of inputs	4

4	Number of output	1
5	Number of MFs	3
6	And method	Prod
7	Or method	Probar
8	Implication	Min
9	Aggregation	Max
10.	Defuzzification	Wtaver
11	Total number of fuzzy rule	81
12	MFs parameters	36
13	Total consequent parameters	405
14	Total parameters	441

4.5. ANFILS three-dimensional surface plot

Figure 10 shows the effect of the interactions of the process variables on percentage removal of naphthalene. Similar trends are observed for adsorption capacity of the composite adsorbent. Figure 10(a) shows the interaction of surfactant concentration, X_1, and activation time, X_2, on the percentage removal of naphthalene. An increase in surfactant concentration shows a corresponding increase in the percentage removal of naphthalene up to a peak of normalized value of 1.2 (i.e., 116 mg/L), before experiencing a slight decrease in the output value and then end up with a constant trend or a plateau. The activation time, X_2, which projected briefly no effect on the percentage removal of naphthalene between 0 and 0.3 min, after which it showed a sharp increment up to 0.5 (i.e., 2.06 h) and then displayed steadily a decrease in the output value before reaching a plateau. Figure 10(b) shows the interactive effect of surfactant concentration, X_1, and activation temperature, X_3, on percentage removal of naphthalene, which is a similar trend to Figure 10(a). However, the surfactant concentration, X_1, exhibited a sharp decrease after the optimum value.

In a similar development in Figure 10(c), the interaction of chitosan dosage, X_4, and surfactant concentration, X_1, depicts a steady increase in the output value up to a peak normalized value of 0.8 (i.e., 5.2 g) and 1.2 (i.e., 116 mg/L) for chitosan dosage and surfactant concentration respectively before recording a steady decline in the percentage removal of naphthalene and formation of plateau. The interaction effect of chitosan dosage, X_4, and activation time, X_2, is depicted in Figure 10(d). It shows that maximum percentage removal of naphthalene is obtained when the chitosan dosage and activation time are 0.8 (i.e., 5.2 g) and 0.5 (i.e., 2.06 h) respectively before achieving a downtrend while Figure 10(e) illustrates the negative effect between the normalized values within the range of 0–0.6 and 0–0.5 for the interaction of activation time, X_2, and activation temperature, X_3, respectively and positive effect on the response variable(s) above 0.6 and 0.5 respectively. Hence, virtual observations from the 3-D plot using the adaptive neuro-fuzzy inference logic system reveal that the process variables values beyond 68 mg/L of surfactant concentration, X_1, 2 h of activation time, X_2, 84ºC of activation temperature, X_3, and 4.4 g of chitosan dosage, X_4, are very sensitive in determining adequately the percentage removal of naphthalene from aqueous using the synthesized chitosan–CTAB–Na bentonite clay matrix.

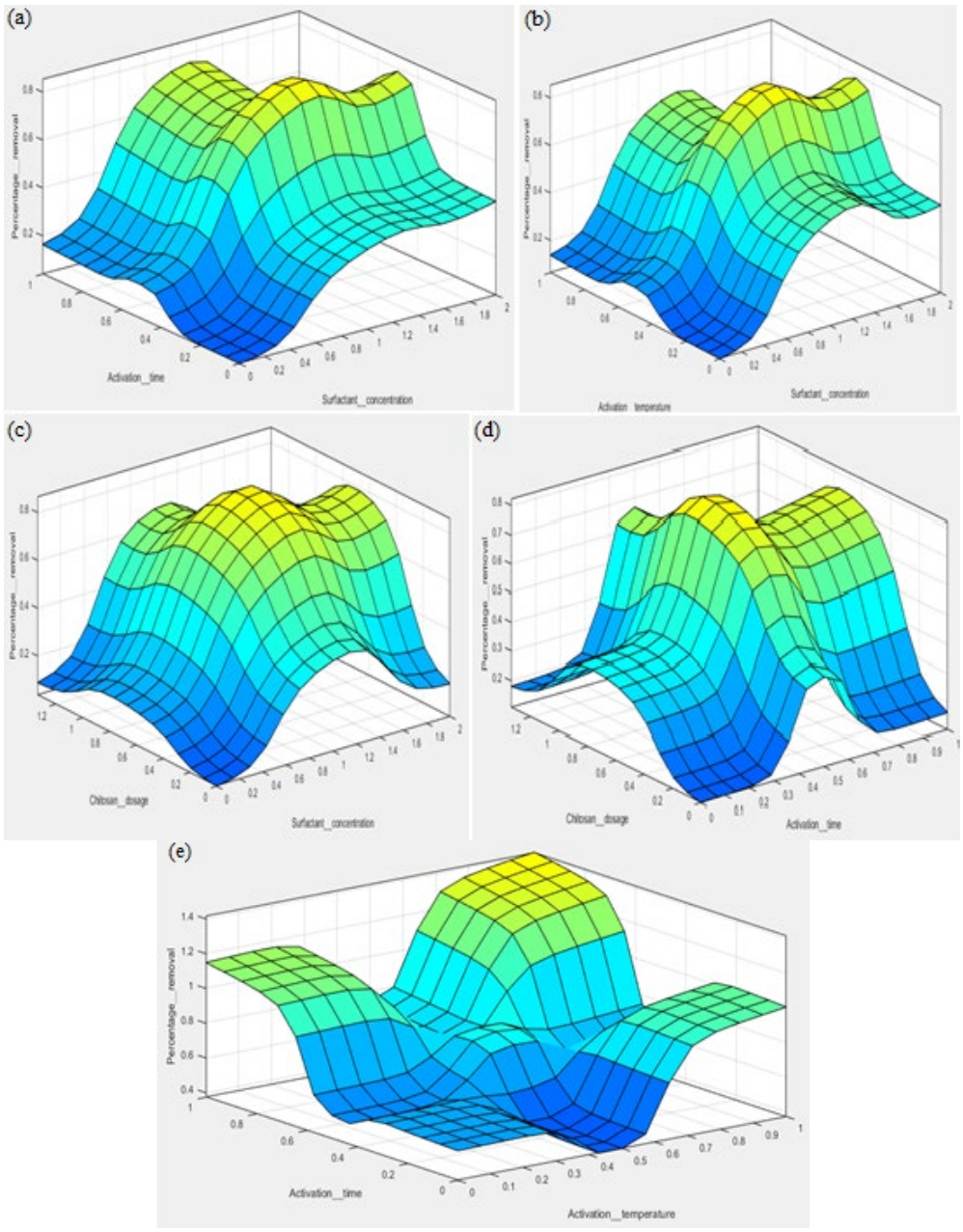

Figure 10. Three-dimensional (a) surfactant concentration, X_1, and activation time, X_2, (b) surfactant concentration, X_1, and activation temperature, X_3, (c) surfactant concentration, X_1, and chitosan dosage, X_4, (d) activation time, X_2, and chitosan dosage, X_4, and (e) activation time, X_2, and activation temperature, X_3, surface plot of the ANFILS model.

4.6. Fitness and comparison of RSM and ANFILS models

The bias, Bi, value was estimated for both responses of % removal of naphthalene and adsorption capacity of the synthesized chitosan–CTAB–Na bentonite clay matrix using Equation (31) [102]:

$$Bi = exp\left[\frac{1}{n}\sum_{i=1}^{n} In\left(\frac{\varphi_{i,e}}{\varphi_{i,p}}\right)\right] \quad (31)$$

The bias values of 0.999785, 1.000281 and 0.999978321 were estimated for percentage removal of naphthalene using RSM, RSM–GA and ANFILS techniques respectively while values of 0.99786, 1.000127 and 0.999978321 were obtained for adsorption capacity of the composite adsorbent using RSM, RSM–GA and ANFILS techniques respectively. The approximated value of 1 for each response translates to the fact that the errors are normally distributed thereby depicting a good model fit [102].

The comparison between the experimental and predicted values of the two responses (i.e., % removal of naphthalene and adsorption capacity of the composite nanoparticles of chitosan–CTAB–Na bentonite clay) using RSM and ANFILS techniques are presented in Table 12 and depicted in Figure 11.

Table 12. Experimental % removal of naphthalene, $(R_e)_{expt}$, and adsorption capacity, $(q_e)_{expt}$, of chitosan–CTAB–Na bentonite clay matrix and their RSM and ANFILS predicted values

$(R_e)_{expt}$ (%)	RSM	ANFILS	$(q_e)_{expt}$ (mg/g)	RSM	ANFILS
	$(R_e)_{pred}$ (%)			$(q_e)_{pred}$ (mg/g)	
79.10	81.0313	79.1000	197.7500	202.5780	197.7500
96.43	93.8050	96.4300	241.0750	234.5110	241.0750
86.67	87.3650	86.6700	216.6750	218.4130	216.6750
97.96	95.8058	97.9600	244.900	239.5150	244.9000
87.81	83.3088	87.8100	219.5250	208.2720	219.5250
95.81	96.0821	95.8100	239.5250	240.2050	239.5250
88.72	89.6430	88.7200	221.8000	224.1060	221.8000
99.62	98.0833	99.6200	249.0500	245.2080	249.0500
84.77	85.5783	84.7700	211.9250	213.9460	211.9250
95.24	94.6092	95.2400	238.1000	236.5230	238.1000
92.39	93.0645	92.3900	230.9750	230.980	230.9750
99.62	96.6104	99.6200	249.0500	241.5260	249.0500
86.72	87.8558	86.7200	216.8000	219.6400	216.8000
99.62	96.8867	99.6200	249.0500	242.2170	249.0500
96.77	94.1896	96.7700	241.9250	235.4740	241.9250
98.72	98.8879	98.7200	246.8000	247.2200	246.8000
82.86	82.1038	82.8600	207.1500	205.2590	207.1500
95.24	99.5754	95.2400	238.1000	248.9390	238.1000
86.77	88.1521	86.7700	216.9250	220.3800	216.9250
94.29	96.4871	94.2900	235.7250	241.2180	235.7250
89.53	90.4721	89.5300	223.8250	226.1800	223.8250
92.39	95.0271	92.3900	230.9750	237.5680	230.9750
87.62	89.3288	87.6200	219.0500	223.3220	219.050
92.81	94.6804	92.8100	232.0250	236.7010	232.0250
96.43	95.6629	95.6629	241.0750	239.1570	239.1573
96.00	95.6629	95.6629	240.0000	239.1570	239.1573
96.43	95.6629	95.6629	241.0750	239.1570	239.1573

97.34	95.6629	95.6629	243.3500	239.1570	239.1573
93.29	95.6629	95.6629	233.225	239.1570	239.1573
96.00	95.6629	95.6629	240.000	239.1570	239.1573
94.15	95.6629	95.6629	235.3750	239.1570	239.1573

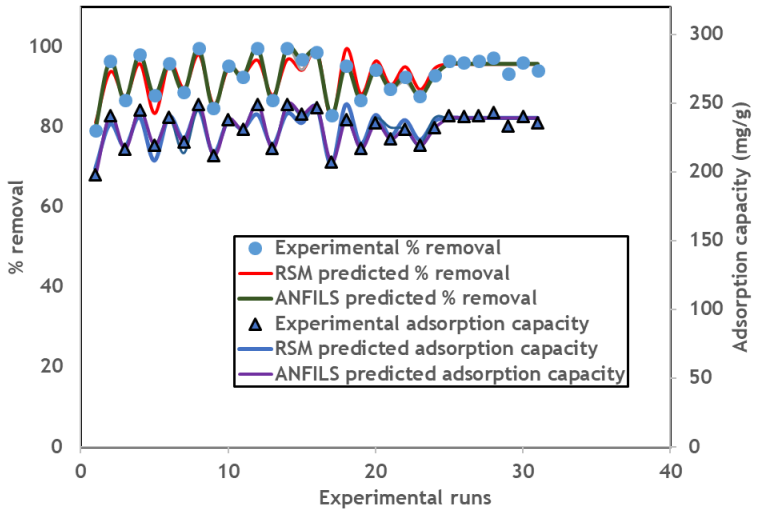

Figure 11. Experimental % removal of naphthalene, $(R_e)_{expt}$, and adsorption capacity, $(q_e)_{expt}$, of chitosan–CTAB–sodium bentonite matrix and their RSM and ANFILS predicted values.

From Table 12, the values of the % mean absolute deviation (MAD) for the % removal of naphthalene using RSM and ANFILS models are computed to be ± 3.7222 and ± 0.0012 respectively. The % MAD values for adsorption capacity of composite nanoparticles of chitosan–CTAB–Na bentonite clay are computed to be $\pm$ 3.8716 and $\pm$ 0.0042 respectively using RSM and ANFILS models respectively. Moreover, the % errors computed for both responses are less than 5% using RSM and ANFILS models It can thus be deduced that both techniques show good modelling abilities of the adsorption data of naphthalene on the prepared composite nanoparticles of chitosan-CTAB-sodium bentonite clay as adsorbent. However, the ANFILS is a better fit model than the RSM for reason of having lower % MAD and % error values than those computed for RSM.

Equally, the error functions, given in Equations (13) to (23), are used to compare the predictive abilities of RSM and ANFILS models. The model with the higher values of *R*, R^2, $adj.R^2$, *WI*, *CI* and *DWT* and the lower values of all other error functions (*RMSE*, *MAE*, *MAPE*, *MPE*, *SPE*, and *TIC*) depicts the better fitted model. According to Silva et al. [89], confidence (or performance) index, $CI > 0.85$ depicts excellent process modeling for both models applied in this study. From the aforementioned statements and values displayed in Table 13, ANFILS is a better fitted model than RSM. Hence, ANFILS model can be applied to the experimental adsorption data of naphthalene on the chitosan–CTAB–sodium bentonite composite nanoparticles as adsorbent than the RSM technique. The ANFIL technique can be reliably applied to the experimental adsorption data of naphthalene on the chitosan–CTAB–sodium bentonite composite nanoparticles. Table 13 shows the values of the error functions for each model.

Table 13. Model error function comparison

Error function	RSM	ANFILS	RSM	ANFILS
	Values of error function in % removal		Values of error function in adsorption capacity	
R^2	0.8640	0.9860	0.864	0.9860
$adj.R^2$	0.8590	0.9850	0.8590	0.9850
RMSE	1.9475	0.6257	4.8642	0.6257
MAE	0.0518	0.0081	0.1283	0.0081
MAPE	1.7368	0.2634	1.7134	0.2634
MPE	5.5907	0.8454	5.5369	0.8454
SPE	2.0984	0.6742	5.2410	0.6742
TIC	0.0105	0.0034	0.0105	0.0034
WI	0.9621	0.9965	0.9622	0.9997
R	0.9319	0.9930	0.9319	0.9930
CI	0.8963	0.9892	0.8967	0.9926
DWT	1.9130	2.3860	2.0030	2.3860

4.7. Optimization of the process variables

The optimal process conditions for the % removal of naphthalene and adsorption capacity of the synthesized composite nanoparticles of chitosan–CTAB–sodium bentonite were carried out using the hybrid of RSM–GA and ANFILS 3–D surface pot optimization techniques in the MATLAB R2018b software environment.

Table 14. Optimized condition for various single and hybrid models

Technique	Process variables model prediction				$(R_e)_{expt}$	$(R_e)_{pred}$	$(q_e)_{expt}$	$(q_e)_{pred}$
	X_1 (mg/L)	X_2 (h)	X_3 (°C)	X_4 (g)	(%)	(%)	(mg/g)	(mg/g)
RSM	97.5768	2.0303	87.8788	3.7778	98.970	100.1060	248.39	250.2651
RSM-GA	79.1444	1.3436	88.7521	3.2416	97.240	96.1602	248.39	265.5082
ANFILS	116.000	2.0600	81.2000	5.2000	99.020	99.055	248.86	248.6375
	% error in % removal				% error in adsorption capacity			
RSM	-1.1478				-0.7549			
RSM-GA	1.1229				0.7492			
ANFILS	-0.0353				0.0894			

Genetic algorithm is a population based probabilistic iterative, search and optimization techniques, which operate on the mechanism and premises of natural genetics and evolution. It is a renowned stochastic search technique that improves performance by its unique ability to locate regions within the purview of any solution space to arrive at optimal solutions beyond the entrapment of local minima which other models use in this article are prone to [88]. The genetic algorithm tool box embedded in MATLAB R2018b software was used for the optimization process at the default settings. By default, genetic algorithms generate minimum values. However, for maximum values of the process variables, the fitness function adopted is usually converted to maximization by inversing or changing the sign [102] and

applying the principle of Pareto analysis especially for multiple variable responses [88]. Equations (28) and (29) were used as the fitness function for the optimization of RSM–GA using multi response genetic algorithm tool box. The fitness value with the least *MSE* value of the response variables alongside the corresponding process variables were selected as the optimum conditions. Table 14 shows the predicted response variables and their respective experimental process variables values for RSM, RSM–GA and ANFILS techniques. The results show good prediction ability of three models. However, ANFILS again portrayed the best having the least percentage errors for both % removal of naphthalene and adsorption capacity of the composite nanoparticles of chitosan–CTAB–sodium bentonite clay.

5. Conclusions

In this study, RSM, RSM–GA and ANFILS 3–D pot optimization techniques were used to model and optimize the conditions for % removal of naphthalene and adsorption capacity of the synthesized chitosan–CTAB–sodium bentonite clay matrix. Although both techniques of RSM and ANFILS showed good modeling abilities of the adsorption data of naphthalene, ANFILS models are better fitted models to both responses investigated than the RSM models for reasons of having lower % MAD of ± 0.0012 and ± 0.0042 for the % removal of naphthalene and adsorption capacity respectively in comparison with the respective values of ± 3.7222 and ± 3.8716 obtained using RSM model. Moreover, higher values of *R*, R^2, $adj.R^2$, *WI*, *CI* and *DWT* and the lower values of all other error functions (*RMSE*, *MAE*, *MAPE*, *MPE*, *SPE*, and *TIC*) were obtained when ANFILS models were applied to the experimental data of naphthalene than when applied to RSM models. The optimal conditions of the design variables and responses were obtained using RSM, RSM–GA and ANFILS 3–D surface pot optimization techniques wherein ANFILS was adjudged the best to predict these conditions. The ANFILS predicted optimal conditions were $X_1 = 116.00$ mg/L, $X_2 = 2.06$ h, $X_3 = 81.2^{o}$C and $X_4 = 5.20$ g and predicted responses were 99.055% removal of naphthalene and 248.6375 mg/g adsorption capacity, which were in excellent agreement with the corresponding experimental values of 99.020% and 248.86 mg/g with % errors of -0.0353 and 0.0894 respectively. Hence, in this study, ANFILS has been successfully used to model and optimize the conditions for the treatment of industrial wastewater containing polycyclic aromatic compounds, especially naphthalene and is hereby recommended for such and similar studies.

Funding statement

This work did not receive any specific grant from funding agencies in the public, commercial or non-profit sector.

Conflict of interest

On behalf of all authors, the corresponding author states that there is no conflict of interest.

References

[1] Alslaibi, T., Abustan, I., Azmier, M., & Foul, A.A. (2013). Cadmium removal from aqueous solution using microwaved olive stone activated carbon. *Journal of Environmental Chemical Engineering*, *1*(3), 89–599. https://doi.org/10.1016/j.jece.2013.06.028

[2] Satouh, S., Martín, J., del Mar Orta, M., Medina-Carrasco, S., Messikh, N., Bougdah, N., Santos, J.L., Aparicio I., & Alonso E. (2021). Adsorption of polycyclic aromatic hydrocarbons by natural, synthetic and modified clays. *Environments*, *8*(11), 124. https://doi.org/10.3390/environments8110124

[3] Darajeh, N., Alizadeh, H., Farraji, H., Park, J., Barghi, A., & Rezania, S. (2020). Removal of polycyclic aromatic hydrocarbon (PAHs) by different physicochemical methods; a mini-review. *Journal of Energy and Environmental Pollution*, *1*(2), 44–50. https://doi.org/10.47277/JEEP/1(2)50

[4] Patel, A.B., Shaikas, S., Jain, K.R., Desai, C., & Madamwar, D. (2020). Polycyclic aromatic hydrocarbons: sources, toxicity and remediation approaches. *Frontiers in Microbiology*, 11:1–23. https://doi.org/10.3389/fmicb.2020.562813

[5] Liu, J.J., Wang, X.C., & Fan, B. (2011). Characteristics of PAH adsorption on inorganic particles and activated sludge in domestic wastewater treatment. *Bioresource Technology*, *102*(9), 5305–5311. https://doi.org/10.1016/j.biortech.2010.12.063

[6] Filho, J.L.A., de Moura, L.G.M., & Ramos, A.C. da S. (2010). Polycyclic aromatic hydrocarbons (PAHs) adsorption on solid surfaces applied to waste lubricant oils recovery process. *The Canadian Journal of Chemical Engineering*, 88, 411–416. https://doi.org/10.1002/cjce.20286

[7] Vhahangwele, M., Mugera, G.W., & Tholiso, N. (2014). Defluorination of drinking water using Al^{3+}–modified bentonite clay: optimization of fluoride adsorption conditions. *Toxicology & Environmental Chemistry*, *96*(9), 1294–1309. https://doi.org/10.1080/02772248.2014.977289

[8] Cabal, B., Budinova, T., Ania, C.O., Tsyntsarski, B., Parra, J.B., & Petrova, B. (2009). Adsorption of naphthalene from aqueous solution on activated carbons obtained from bean pods. *Journal of Hazardous Materials*, *161*(2– 3) , 1150–1156. https://doi.org/10.1016/j.jhazmat.2008.04.108

[9] Yuan, M.J., Tong, S.T., Zhao, S.Q., & Jia, C.Q. (2010). Adsorption of polycyclic aromatic hydrocar-bons from water using petroleum coke-derived porous carbon. *Journal of Hazardous Materials*, *181*(1– 3), 1115–1120. https://doi.org/10.1016/j.jhazmat.2010.05.130

[10] Iovino, P., Canzano, S., Capasso, S., Di Natale, M., Erto, A., Lama, A., & Musmarrab, D. (2013). Single and competitive adsorption of toluene and naphthalene onto activated carbon. *Chemical Engineering Transactions*, 32, 67–72. https://doi.org/10.3303/CET1332012

[11] Liu, D., Wu, Z., Ge, X., Cravotto, G., Wu, Z., & Yan, Y. (2016). Comparative study of naphthalene adsorption on activated carbon prepared by microwave-assisted synthesis from different typical coals in Xinjiang. *Journal of the Taiwan Institute of Chemical Engineers*, 59, 563–568. https://doi.org/10.1016/j.jtice.2015.09

[12] Patiño-Ruiz, D.A., De Ávila, G., Alarcón-Suesca, C., González-Delgado, Á.D., & Herrera, A. (2020). Ionic cross-linking fabrication of chitosan-based beads modified with FeO and TiO_2 nanoparticles: adsorption mechanism toward naphthalene removal in seawater from Cartagena bay area. *ACS Omega*, *5*(41), 26463–26475. https://doi.org/10.1021/acsomega.0c02984

[13] Kumari, N., & Mohan, C. (2021). Basis of clay minerals and their characteristics properties. *Intech Open*, 1–29. http://dx.doi.org/10.5772/intechOpen.97672

[14] Monvisade, P., & Siriphannon, S. (2009). Chitosan intercalated Montmorillonite: preparation, characterization and cationic dye and adsorption. *Applied Clay Science*, *42*(3–4), 427–431. https://doi.org/10.1016/j.clay.2008.04.013

[15] Teofilović, V., Pavličević, J., Bera, O., Jovičić, M., Simendić, J.B., Szécsényi, K.M., & Aroguz, A.A. (2014). The preparation and thermal properties of chitosan/bentonite composite beads. *Hemijska Industrija*, *68*(6), 653–659. https://doi.org/10.2298/HEMIND130905088T

[16] Savitri, E. & Budhyantoro, A. (2017.) The effect of ratio chitosan-bentonite and processing time on the characterization of chitosan-bentonite composite. *IOP Conference Series: Material Science and Engineering*, 223, 012034. https://doi.org/10.1088/1757-899x/223/1/012034

[17] Jia, J., Liu, Y., & Sun, S. (2021). Preparation and characterization of chitosan/bentonite composites for Cr (VI) removal from aqueous. *Adsorption Science & Technology*, 6681486, 1–15. https://doi.org/10.1155/2021/6681486

[18] Tanhaei, B., Esfandyari, M., Ayati, A., & Sillanpää, M. (2017). Neuro-fuzzy modelling of adsorptive performance of magnetic chitosan nanocomposite. *Journal of Nanostructure in Chemistry*, 7, 29–36. https://doi.org/10.1007/s40097-016-0211-4

[19] Suitana, S., Karmaker, B., Saifullah, A.S.M., Uddin, M.G., & Moniruzzaman, M. (2022). Environmental-friendly clay coagulant aid for wastewater treatment. *Applied Water Science*, 12, 1–10. https://doi.org/10.1007/s13201-021

[20] Damian, G., Damian, F., Szakacs, Z., Lepure, G., & Astefanei, D. (2021). Mineralogical and physico-chemical characterization of the Orasu-Nou (Romania) bentonite resources. *Minerals*, *11*(9), 1–19. https://doi.org/10.3390/min11090938

[21] Oliveira, C.I.R., Rocha, M.C.G., Silva, A.L.N., & Bertolino, L.C. (2016). Characterization of bentonite clays from Cubati, Paraiba (Northeast of Brazil). *Ceramica*, *62*(363), 272–277. https://dx.doi.org/10.1590/0366-69132016623631970

[22] Shah, L.A., Khattak, N.S., Valenzuela, M.G.S., Manan, A., & Diaz, F.R.V. (2013). Preparation and characterization of purified Na-activated bentonite from Karak (Pakistan) for pharmaceutical use. *Clay Minerals*, *48*(4), 595–603. https://doi.org/10.1180/claymin.2013.048.4.03

[23] Miyoshi, Y., Tsukimura, K., Morimoto, K., Suzuki, M., & Takagi, T. (2018). Comparison of methylene blue adsorption on bentonite measured using the spot and colorimetric methods. *Applied Clay Science*, 151, 140–147. https://dx.doi.org/10.1016/j.clay.2017.10.023

[24] Samiey, B., Cheng, C.H., & Wu, J. (2014). Organic-inorganic hybrid polymers as adsorbents for removal of heavy metals ions from solution: A review. *Materials*, *7*(2), 673–726. https://doi.org/10.3390/ma7020673

[25] Pandey, P., & De, N. (2018). Surfactant-induced changes in physicochemical characters of bentonite clay. *International Research Journal of Pure and Applied Chemistry*, *15*(4), 1–11. https://doi.org/10.9734/IRJPAC/2017/39374

[26] Rihayat, T., Satriananda, S., Riskina, S., Syahputra, W., & Mawaddah, N. (2019). Formulation of Polyurethane with bentonite-chitosan as filler applied to carbon steel as an antibacterial and environmentally friendly paint. *IOP Conference Series: Material Science and Engineering*, 536, 1–9, https://doi.org/10.1088/1757-899X/536/1/012093

[27] Rittirong, K., Uasopon, S., Prachayawasin, P., Euaphantasate, N., Aiempanakit, K., & Ummartyotin, S. (2015). CTAB as a soft template for modified clay as filler in active packaging. *Data in Brief*, 3, 47–50. https://dx.doi.org/10.1016/j.dib.2015.02.002

[28] Zohra, B., Aicha, K., Fatima, S., Nourredine, B., & Zoubir, D. (2008). Adsorption of direct red 2 on bentonite modified by cetyltrimethylammonium bromide. *Chemical Engineering Journal*, *136*(2–3), 295–305. https://doi.org/10.1016/j.cej.2007.03.086

[29] Betiku, E., Odude, V.O., Ishola, N.B., Bamimore, A., & Osunleke, A.S. (2016). Predictive capability evaluation of RSM, ANFIS and ANN: a case of reduction of high free fatty acid of palm kernel oil via esterification process. *Energy Conversion and Management*, 124, 219–230. http://dx.doi.org/10.1016/j.enconman.2016.07.030

[30] Giannakas, A. & Pissanou, M. (2018). Chitosan/bentonite nanoparticles for waste water treatment: A review. *Science Forecast Journal of Nanochemistry and Nanotechnology*, *1*(1), 1–18.

[31] Liu, Q., Yang, B., Zhang, L., & Huang, R. (2015). Adsorption of an anionic azo dye by cross-linked chitosan/bentonite composite. *International Journal of Biological Macromolecules, 72,* 1129–1135. https://doi.org/10.1016/j.ijbiomac.2014.10.008

[32] Senol, Z.M. & Simsek, S. (2022). Insights into effective adsorption of lead ions from aqueous solution by using chitosan-bentonite composite beads. *Journal of Polymer and Environment*. https://doi.org/10.1007/s10924-022-02464-8

[33] Huang, R., Liu, Q., Zhang, L., & Yang, B. (2014). Utilization of cross-linked chitosan/bentonite composite in the removal of methyl orange from aqueous solution. Water Science and Technology, *71*(2), 174–182. http://dx.doi.org/10.2166/wst.2014.478

[34] Chen, H., Zheng, K., Zhu, A., Meng, Z., Li, W. & Qin, C. (2020). Preparation of bentonite/chitosan composite for bleaching of deteriorating transformer oil. Polymers, *12* (60). https://doi.org/10.3390/polym12010060

[35] Jia, J., Liu, Y. & Sun, S. (2021). The preparation and characterization of chitosan/bentonite composites for Cr (VI) removal from aqueous solutions, *Adsorption Science and Technology*, *2021* (6681486), 1–15. https://doi.org/10.1155/2021/6681486

[36] Huang, R., Zhang, L., Hu, P., & Wang, J. (2016). Adsorptive removal of Congo red from aqueous solutions using crosslinked chitosan and crosslinked chitosan immobilized bentonite. *International Journal of Biological Macromolecules, 86, 496–504.* http://dx.doi.org/10.1016/j.ijbiomac.2016.01.083

[37] Zhang, L., Hu, P., Wang, J., & Huang, R. (2016). Crosslinked quaternized chitosan/bentonite composite for the removal of Amino black 10B from aqueous solutions.*International Journal of Biological Macromolecules, 93,* 217–225. http://dx.doi.org/10.1016/j.ijbiomac.2016.08.018

[38] Dotto, G.L, Rodrigues, F.K, Tanabe EH, Frohlich, R., Bertuol, D.A., Martins, T.R. & Foletto, E.L. (2016). Development of chitosan/bentonite hybrid composite to remove hazardous anionic and cationic dyes from colored effluents. Journal of Environmental Chemical Engineering. 4, 3230–3239. http://dx.doi.org/10.1016/j.jece.2016.07.004

[39] Ngah, W. W.S., Ariff, N.F.M. & Hanafiah, M.A.K.M (2010). Preparation, Characterization, and Environmental Application of Crosslinked Chitosan-Coated Bentonite for Tartrazine Adsorption from Aqueous Solutions. *Water Air Soil Pollut*ion, 206, 225–236. https://doi.org/10.1007/s11270-009-0098-5

[40] Ngah, W. W. S., Ariff, N. F. M., Hashim, A., & Hanafiah, M. A. K. M. (2010). Malachite Green Adsorption onto Chitosan Coated Bentonite Beads: Isotherms, Kinetics and Mechanism. *CLEAN - Soil, Air, Water, 38*(4), 394–400. https://doi.org/10.1002/clen.200900251

[41] Hariani, P.L, Fatma, F., Riyanti, F. & Ratnasari, H. (2015). Adsorption of Phenol Pollutants from Aqueous Solution Using Ca-Bentonite/Chitosan Composite. *Jurnal Manusia Dan Lingkungan*, *22*(2), 233–239. https://doi.org/10.22146/jml.18747

[42] De Luna, M. D. G., Futalan, C. M., Jurado, C. A., Colades, J. I., & Wan, M.-W. (2017). Removal of ammonium-nitrogen from aqueous solution using chitosan-coated bentonite: Mechanism and effect of operating parameters. *Journal of Applied Polymer Science, 135*(9), 45924. https://doi.org/10.1002/app.45924

[43] Guo, J., Chen, S., Liu, L., Li, B., Yang, P., Zhang, L., & Feng, Y. (2012). Adsorption of dye from wastewater using chitosan–CTAB modified bentonites. *Journal of Colloid and Interface Science, 382*(1), 61–66. https://doi.org/10.1016/j.jcis.2012.05.044

[44] Bulut, Y., & Karaer, H. (2014). Removal of methylene blue from aqueous solution by crosslinked chitosan-g-poly(acrylic acid)/bentonite composite. *Chemical Engineering Communications, 202*(12), 1635–1644. http://dx.doi.org/10.1080/00986445.2014.968713

[45] Huang, R., Zheng, D., Yang, B., Wang, B., & Zhang, Z. (2011). Preparation and characterization of CTAB-HACC bentonite and its ability to adsorb phenol from aqueous solution. *Water Science and Technology, 64*(1), 286–292. https://doi.org/10.2166/wst.2011.582

[46] Shakib, F., Dadvand Koohi, A., & Kamran Pirzaman, A. (2017). Adsorption of methylene blue by using novel chitosan-g-itaconic acid/bentonite nanocomposite – equilibrium and kinetic study. *Water Science and Technology, 75*(8), 1932–1943. https://doi.org/10.2166/wst.2017.077

[47] Wang, J., Liu, Y., Hu, P., & Huang, R. (2017). Adsorption of phosphate from aqueous solution by Zr(IV)-crosslinked quaternized chitosan/bentonite composite. *Environmental Progress & Sustainable Energy, 37*(1), 267–275. https://doi.org/10.1002/ep.12667

[48] Osman, N.H., Mazu, N.N., Chyi, J.L.Y., Ramli, M.M., Majid, M.A.H.M.A.M. & Mazlan, H.I. (2021). Chitosan-bentonite crosslinked film as indicator for copper (II) ions adsorption. *European Physical Journal – Applied Physics*, *95*(1), 10401–10408. https://doi.org/10.1051/epjap/2021210089

[49] Huang, C., Huang, Y., Xie, T., Yu, W., & Ai, S. (2021). Adsorption mechanism of bentonite with dispersed chitosan for cadmium ions. Chemical Engineering & Technology, *44*(3), 441–448. https://doi.org/10.1002/ceat.202000505

[50] Xu, X., Cheng, Y., Wu, X., Fan, P. & Scry, R. (2020). Lab (III)-bentonite/chitosan composite: A new type of adsorbent for rapid removal of phosphate from water bodies. Applied Clay Science, *190*(105547), 1–9. https://doi.org/10.1016/j.clay.2020.105547

[51] Lin, Z., Yang, Y., Liang, Z., Zeng, L., & Zhang, A. (2021). Preparation of chitosan/calcium alginate/bentonite composite hydrogel and its heavy metal adsorption properties, Polymers, *13*(1891), 1–19. https://doi.org/10.3390/polym13111891

[52] Aydar, A.Y. (2018). Utilization of response surface methodology, optimization of extraction of plant materials. *Intech Open*, 10, 2–15. https://doi.org/10.5772/intechopen.73690

[53] Biswas, S., Bal, M., Behera, S.K., Sen, T.K., & Meikap, B.C. (2019). Process optimization study of Zn^{+2} adsorption on biochar-alginate composite adsorbent by response surface methodology (RSM). *Water*, *11*(2), 325. https://doi.org/10.3390/w11020325

[54] Rao, J.H., King, P., & Kumar, Y.P. (2018). Application of response surface methodology for optimization of cadmium adsorption in an aqueous solution by activated carbon prepared from *Bauhinia Purpurea* leaves. *Rasayan Journal of Chemistry*, 11(4), 1577–1586. http://dx.doi.org/10.31788/RJC.2018.1144024

[55] Ani, J.U., Okoro, U.C., Aneke, L.E., Onukwuli, O.D., Obi, I.O., Akpomie, K.G., & Ofomatah, A.C. (2019). Application of response surface methodology for optimization of dissolved solids adsorption by activated coal. *Applied Water Science*, 9, 1–11. https://doi.org/10.1007/s13201-0.19-0943-7

[56] Yu, A., Liu, Y., Li, X., Yang, Y., Zhou, Z., & Liu, H. (2021). Modeling and optimization of NH4+ removal from storm water by coal-based granular activated carbon using RSM and ANN coupled with GA. *Water*, *13*(5), 2–22. https://doi.org/10.3390/w13050608

[57] Sarkar, J., Prottoy, Z.H., Bari, M.T., & Al Faraque, M.A. (2021). Comparison of ANFIS and ANN modelling for predicting the water absorption behaviour of polyurethane treated polyester fabric. *Heliyon*, *7*(9), 1–9. https://doi.org/10.1016/j.heliyon.2021.e08000

[58] Okwu, M.O., & Adetunji, O. (2018). A comparative study of artificial neural network (ANN) and adaptive neuro-fuzzy inference system (ANFIS) models in distribution systems with deterministic inputs. *International Journal of Engineering Business Management*, *10*(12), 1–17. https://doi.org/10.1177/1847979018768421

[59] Taher, A.S., Zhou, J., Shen, X., Yin, Y., & Ji, X. (2019). Comparison of RSM with ANFIS in predicting tensile strength of dissimilar friction stir welded AA2024-AA5083 aluminum alloys. *Procedia Manufacturing*, 37, 555–562. https://doi.org/10.1016/j.promfg.2019.12.088

[60] Shivakoti, I., Rodrigues, L.L.R., Cep, R., Pradhan, P.M., & Sharma, A. (2020). Experimental Investigation and ANFIS-based modelling during machining of EN31 alloy steel. *Materials*, *13*(14), 1–15. https://doi.org/10.3390/ma13143137

[61] Mishra, R., Prasad, S.R., & Kumar, S. (2021). ANFIS model to predict effect of tool pin length and position on tensile strength of friction stir welded joint. *Welding International*, 1-10. https://doi.org/10.1080/09507116.2021.1917972

[62] Chainarong, S., Srichok, T., Pitakaso, R., Sirirak, W., Khonjun, S., & Akararungruangku, R. (2021). Variable neighborhood strategy adaptive search for optimal parameters of SSM-ADC 12 aluminum friction stir welding. *Processes*, *9*(10), 1–24.

[63] Mokarram, M., Amin, H., & Khosravi, M.R. (2019). Using adaptive neuro-fuzzy inference system and multiple linear regression to estimate orange taste. *Food Science & Nutrition*, *7*(10), 3176–3184. https://doi.org/10.1002/fsn3.1149

[64] Ghaedi, M., Hosaininia, R., Ghaedi, A.M., Vafaei, A., & Taghizadeh F. (2014). Adaptive neuro-fuzzy inference system model for adsorption of 1,3,4-thiadiazole-2,5-dithiol onto gold nanoparticles-activated carbon. *Spectrochimica Acta Part A: Molecular and Biomolecular Spectroscopy*, 131, 606–614. https://doi.org/10.1016/j.saa.2014.03.055

[65] Mandal, S., Mahapatra, S., & Patel, R.K. (2015). Neuro fuzzy approach for arsenic (III) and chromium (VI) removal from water. *Journal of Water Process Engineering*, 5, 58–75. https://doi.org/10.1016/j.jwpe.2015.01.002

[66] Rebouh, S., Bouhedda, M., & Hanini, S. (2015). Neuro-fuzzy modeling of Cu(II) and Cr(VI) adsorption from aqueous solution by wheat straw. *Desalination and Water Treatment*, 57, 6515–6530. https://doi.org/10.1080/19443994.2015.1009171

[67] Chittoo, B.S., & Sutherland, C. (2019). Adsorption using lime-iron sludge–encapsulated calcium alginate beads for phosphate recovery with ANN- and RSM-optimized encapsulation. *Journal of Environmental Engineering*, *145*(5), 04019019. https://doi.org/10.1061/(asce)ee.1943-7870.0001519

[68] Olafadehan, O.A., Bello, V.E., & Amoo, K.O. (2022). Production and characterization of composite nanoparticles derived from chitosan, CTAB and bentonite clay. *Chemical Papers*. https://doi.org/10.1007/s11696-022-02228-7

[69] Saini, S., Chawla, J., Kumar, R., & Kaur, I. (2019). Response surface methodology (RSM) for optimization of cadmium ions adsorption using $C_{16\text{-}6\text{-}16}$ incorporated mesoporous MCM-41. *SN Applied Sciences*, *1*(8), 894. https://doi.org/10.1007/s42452-019-0922-5

[70] Mourabet, M., El Rhilassi, A., Ziatni, M.B., & Taitai, A. (2014). Comparative study of artificial neural network and response surface methodology for modelling and optimization the adsorption capacity of fluoride onto apatitic tricalcium phosphate. *Universal Journal of Applied Mathematics*, *2*(2), 84–91. https://doi.org/10.13189/ujam.2014.020202

[71] Bayuo, J., Abukari, M.A., & Pelig-Ba, K.B. (2020). Optimization using central composite design (CCD) of response surface methodology (RSM) for biosorption of hexavalent chromium from aqueous media. *Applied Water Science*, *10*(135), 1–12. https://doi.org/10.1007/s13201-020-01213-3

[72] Gaitonde, V.N., Karnik, S.R., Achyutha, B.T. & Siddeswarappa, B. (2005). GA applications to RSM based models for burr size reduction in drilling, *Journal of Scientific and Industrial Research*, *64*(1), 347–353.

[73] Bello, V.E., & Olafadehan, O.A. (2021). Comparative investigation of RSM and ANN for multi-response modeling and optimization studies of derived chitosan from *Archachatina marginata* shell. *Alexandria Engineering Journal*, *60*(4), 3869–3899. https ://doi.org/10.1016/j.aej.2021.02.047

[74] Baghban, A., & Ebadi, T. (2019). GA-ANFIS modeling of higher heating value wastes: application to fuel upgrading. *Energy Sources, Part A: Recovery, Utilization, and Environmental Effects*, *41*(1), 7–13. https://doi.org/10.1080/15567036.2017.1344746

[75] Al-hmouz, A., Shen, J., Al-hmouz, R., & Yang, J. (2012). Modeling and simulation of an adaptive neuro fuzzy inference system (ANFIS) for mobile learning. *IEEE Transactions on Learning Technologies*, *5*(3), 226–237. https://doi.org/10.1109/TLT.2011.36

[76] Calp, M.H. (2019). A hybrid ANFIS-GA approach for estimation of regional rainfall amount. *Gazi University Journal of Science*, 32, 142–162. e-ISSN: 2147-1762

[77] Buragohain, M. (2009). *Adaptive network based fuzzy inference system (ANFIS) as a tool for system identification with special emphasis on training data minimization*, PhD Thesis, Department of Electronics and Communication Engineering, Indian Institute of Technology, Guwahati.

[78] Abdulshahed, A.M., Longstaff, A.P., & Fletcher, S. (2015). The application of ANFIS prediction models for thermal error compensation on CNC machine tools. *Applied Soft Computing*, 27, 158–168. http://dx.doi.org/10.1016/j.asoc.2014.11.012

[79] Mohadesi, M., & Aghel, B. (2020). Use of ANFIS/genetic algorithm and neural network to predict inorganic indicators of water quality. *Journal of Chemical and Petroleum Engineering*, 54, 155–164. https://doi.org/10.22059/jchpe.2020.264471.1244

[80] Kumar, R., & Hynes, N.R.J. (2020). Prediction and optimization of surface roughness in thermal drilling using integrated ANFIS and GA approach. *Engineering Science and Technology, An International Journal*, *23*(1), 30–41. https://doi.org/10.1016/j.jestch.2019.04.011

[81] Biu, D.T., Khosravi, K., Li, S., Shahabi, H., Panahi, M., Singh, V.P., Chapi, K., Shirzadi, A., Panahi, S., Chen, W., & Ahmad, B.B. (2018). New hybrids of ANFIS with several optimization algorithms for flood susceptibility modeling. *Water*, *10*(9), 1210. https://doi.org/10.3390/w10091210

[82] El-Hasnony, I.M., Barakat, S.I., & Mostafa, R.R. (2020). Optimized ANFIS model using hybrid metaheuristic algorithm for Parkinson's disease prediction in IoT environment. *IEEE Access*, 8, 119252–119270. https://doi.org/10.1109/access.2020.3005614

[83] Safihulla, M.A. (2019). *Modeling of optimized neuro-fuzzy logic based active vibration control method for automotive suspension*, M. Sc. Thesis, Grand Valley State University, Michigan, USA.

[84] Khoshnevisan, B., Rafiee, S., Omid, M., & Mousazadeh, H. (2014). Development of an intelligent system based on ANFIS for predicting wheat grain yield on the basis of energy inputs. *Information Processing in Agriculture*, *1*(1), 1–9. http://dx.doi.org/10.1016/j.inpa.2014.04.001

[85] Bello, E.V., & Olafadehan, O.A. (2022). Evaluation of heterocyclic aromatic compound dye (methylene blue) on chitosan adsorbent sourced from African snail shell: Modelling and optimization studies. Journal of Applied Science and Process Engineering, 9 (1), 1054-1090. https://doi.org/10.33736/jaspe.4464.2022

[86] Onu, C.E., Igbokwe, K.P., Nwabame, T.J., Nwajinka, C.O., & Ohale, P.E. (2020). Evaluation of optimization techniques in predicting optimum moisture content reduction in drying potatoes slices. *Artificial Intelligence in Agriculture*, 4, 39–47. https://doi.org/10.1016/j.aiia.2020.04.001

[87] Bello, V.E., & Olafadehan, O.A. (2021). Comparative investigation of RSM and ANN for multi-response modeling and optimization studies of derived chitosan from *Archachatina marginata* shell. *Alexandria Engineering Journal*, *60*(4), 3869–3899. https ://doi.org/10.1016/j.aej.2021.02.047

[88] Olafadehan, O.A. (2021). *Fundamentals of Adsorption Processes*, LAP Lambert Academic Publishing, OmniScriptum DUE GmbH.

[89] Silva, G.N., Tomaz, R.S., Sant'anna, I.C., Carneiro, V.Q., Cruz, C.D., & Nascimento, M. (2016). Evaluation of the efficiency of artificial neural networks for genetic value prediction. *Genetic Molecular Research*, *15*(1):1–11. https://doi.org/10.4328/gmr.15017676

[90] Yaseen, Z.M., Ebtehaj, I., Kim, S., Sanikham, H., Asadi, H., Ghareb, M.I., Bonakdari, H., Montar, W.H.M.W., Al-Ansari, N., & Shahid, S. (2019). Novel hybrid data-intelligence model for forecasting monthly rainfall with uncertainty analysis. *Water, 11*(3), 1–23. https://doi.org/10.3390/w11030502

[91] Shahbeig, H., Bagheri, N., Ghorbanian, S.A., Hallajisani, A., & Poorkarimi, S. (2013). A new adsorption isotherm model of aqueous solutions on granular activated carbon. *World Journal of Modelling and Simulation*, *9*(4), 243–254.

[92] Sabreena, A.H.N., Azma, Y.N., & Mohamad, O. (2016). Response surface methodology for optimization of parameters for extraction of stevia rebaudiana using water, H_2O. *IIOABJ*, *7*(1), 459–466.

[93] Zhou, Q., Ding, L., Zhu, Y., Zhong, M., & Yang, C. (2020). Process parameters optimization of gallic acid removal from water by MIEX resin based on response surface methodology. *Processes*, *8*(3), 1–11. https://doi.org/10.3390/pr8030273

[94] Kalavathy, M.H., Regupathi, I., Pillai, M.G., & Miranda, L.R. (2009). Modelling, analysis and optimization of adsorption parameters for H_3PO_4 activated rubber and saw dust using response surface methodology (RSM). *Colloids and Surfaces B: Biointerfaces*, *70*(1), 35–45. https://doi.org/10.1016/j.colsurfb.2008.12.007

[95] Chittoo, B.S., & Sutherland, C. (2019). Column breakthrough studies for the removal and recovery of phosphate by lime-iron sludge: Modelling and optimization using artificial neural network and adaptive neuro-fuzzy inference system. *Chinese Journal of Chemical Engineering*, *28*(7), 1847–1859. https://doi.org/10.1016/j.cjche.2020.02.022

[96] Trinh, T.K., & Kang, L.S. (2010). Application of response surface method as an experimental design to optimize coagulation tests. *Environmental Engineering Research*, *15*(2), 063–070. https://doi.org/10.4491/eer.2010.15.2.063

[97] Supeni, E.E., Epaarachchi, J.A., Islam, M.M., & Lau, K.T. (2014). Development of artificial neural network model in predicting performance of the smart wind turbine blade. *Journal of Mechanical Engineering and Sciences*, 6, 734–745. http://dx.doi.org/10.15282/jmes.6.2014.1.0071

[98] Igwe, J.E., & Agu, C.S. (2016). Improvement of waste plastic plant from crude oil recovery. *American Journal of Engineering Research*, *5*(8), 98–104. e-ISSN: 2320-0847

[99] Elbaz, K., Shen, S.L., Zhou, A., Yuan, D.J., and Xu, Y. (2019). Optimization of EPB shield performance with adaptive neuro-fuzzy inference system and genetic algorithm. *Applied Science*, *9*(4), 2–17. https://doi.org/10.3390/app9040780

[100] Liu, P., Leng, W., & Fang, W. (2013). Training ANFIS model with an improved quantum-behaved particle swarm optimization algorithm. *Mathematical Problem in Engineering*, *2013*(1), 1–7. https://doi.org/10.1155/2013/595639

[101] Kumar, R.V., Moorthy, I.G., & Pugazhenthi, G. (2015). Modeling and optimization of critical parameters by hybrid RSM-GA for the separation of BSA using tubular configured MFI-type zeolite microfiltration membrane. *RSC Advances*, *5*(106), 1–44. https://doi.org/10.1039/C5RA20114D

[102] Kalathinga, M.S.H., Basak, S., & Mitra, J. (2019). Artificial neural network modelling and genetic algorithm optimization of process parameters in fluidized bed drying of green tea leaves. *Journal of Food Process Engineering*, *43*(1), 1–7. https://doi.org/10.1111/jfpe.13128w11030502